AFFIDAVIT

I declare that I have authored this thesis independently, that I have not used other than the declared sources/resources, and that I have explicitly indicated all material which has been quoted either literally or by content from the sources used. The text document uploaded to TUGRAZonline is identical to the present master's thesis.

_____
Date

_____
Signature

Abstract

In recent years many research was done in finding alternatives for silicon solar cells. Emerging photovoltaic technologies like perovskite thin-film solar cells, nanocomposite solar cells and quantum-dot sensitized solar cells have drawn the interest. Polymer/nanocrystal solar cells, which are a type of nanocomposite solar cells, are a combination of an organic, conjugated polymer and inorganic nanocrystals and connect the advantages of both materials in one system. Quantum-dot sensitized solar cells are an advancement of the dye-sensitized solar cell and use nanocrystals instead of a dye for light-harvesting. A big advantage of the use of nanocrystals is the possibility of tuning their optical and electronic properties by changing their size and shape.

In this thesis $CuInS_2$ nanocrystals were prepared via colloidal methods and the hot-injection method, respectively, using different copper and indium precursors, sulfur sources or molecular precursors (e.g. metal xanthates) and capping agents. The synthesized nanocrystals were characterized by X-ray diffraction measurement, transmission electron microscopy and UV/Vis spectroscopy.

The long-chained, insulating capping agents, which stabilize but insulate the nanocrystals, were exchanged by shorter ligands. The ligand exchange was conducted with 1-hexanethiol and ammonium thiocyanate and the ligand exchange was analyzed by infrared spectroscopy and thermogravimetric analysis. In both cases the success of the ligand exchange was proven.

The 1-hexanethiol capped nanocrystals were used as acceptor phase in nanocomposite solar cells in which the polymer poly[N-9'-heptadecanyl-2,7-carbazole-alt-5,5-(4',7'-di-2-thienyl-2',1',3'-benzothiadiazole)] (PCDTBT) was used as donor phase. Solar cells were prepared in the bulk heterojunction assembly. For the optimization of the solar cells various ratios of polymer to nanocrystals as well as annealing steps were tested. Out of the investigated ratios a polymer to CIS ratio of 1:9 proved to be the best.

The thiocyanate capped nanocrystals were used as light absorber in quantum-dot sensitized solar cells. Different polymers were tested for their suitability as hole transport layer when using $CuInS_2$ nanocrystals. The influence of annealing and a treatment with $InCl_3$ was investigated. The combination of a single layer of $CuInS_2$ nanocrystals and the polymer poly(3-hexylthiophene-2,5-diyl) (P3HT) used as hole transport layer provided the highest values of the characteristic parameters of the solar cells.

The solar cells were characterized by UV/Vis spectroscopy, surface profiler measurements, photoluminescence quenching experiments, current-voltage curves and external quantum efficiency spectra.

Kurzfassung

Während der den letzten Jahren wurde viel an Alternativen für Siliziumsolarzellen geforscht. Alternative Photovoltaik Technologien wie zum Beispiel Perowskit Dünnschichtsolarzellen, Nanocomposit Solarzellen und Quantendot-Solarzellen weckten das Interesse. Polymer/Nanokristall Solarzellen, welche zu den Nanocompositsolarzellen gehören, verwenden eine Kombination von einem organischen, konjugiertem Polymer und anorganischen Nanokristallen und verbinden die Vorteile beider Materialien in einem System. Quantendot-sensibilisierte Solarzellen stellen eine Weiterentwicklung der Farbstoffsolarzelle (Grätzelzelle) dar und verwenden statt des lichtempfindlichen Farbstoffes Nanokristalle zur Absorption des Lichts. Ein großer Vorteil der Verwendung von Nanokristallen ist die Möglichkeit, dass deren optischen und elektronischen Eigenschaften durch deren Größe und Form beeinflusst werden können.

In dieser Arbeit wurden $CuInS_2$ Nanokristalle über kolloidale Methoden und der Hot-Injection Methode hergestellt. Verschiedene Kupfer- und Indiumprecursor, Schwefelquellen oder molekulare Precursor (zB Metallxanthate) und Liganden wurden verwendet. Die synthetisierten Nanokristalle wurden mittels Röntgendiffraktometrie, Transmissionselektronenmikroskopie und UV/Vis Spektroskopie charakterisiert.

Die langkettigen, isolierenden Liganden, welche die Nanokristalle stabilisieren, aber auch isolieren, wurden durch kürzere Liganden ausgetauscht. Der Ligandenaustausch wurde mit 1-Hexanthiol und Ammoniumthiocyanat durchgeführt. Die Ligandenhülle wurde mittels Infrarotspektroskopie und Thermogravimetrischer Analyse analysiert. In beiden Fällen konnte ein erfolgreicher Ligandenaustausch nachgewiesen werden.

Die mit 1-Hexanthiol stabilisierten Nanokristalle wurden als Akzeptor in Nanocompositesolarzellen verwendet, wo das Polymer Poly[N-9'-heptadecanyl-2,7-carbazole-alt-5,5-(4',7'-di-2-thienyl-2',1',3'-benzothiadiazole)] (PCDTBT) als Donor fungierte. Die Solarzellen wurden im Bulk-Heterojunction-Aufbau gefertigt. Für die Optimierung der Solarzellen wurden verschiedene Verhältnisse von Polymer zu Nanokristallen sowie der Einfluss von Wärmebehandlung getestet. Ein Verhältnis von Polymer zu Nanokristallen von 1:9 stellten sich als am besten heraus.

Die mit Thiocyanat stabilisierten Nanokristalle wurden als Lichtabsorber in Quantendot-sensibilisierten Solarzellen eingesetzt. Verschiedene Polymere wurden auf ihre Eignung als Lochtransportschicht bei der Verwendung von $CuInS_2$ Nanokristallen getestet. Der Einfluss von Tempern und einer Behandlung mit $InCl_3$ wurde untersucht. Die Kombination von nur einer Schicht von $CuInS_2$ Nanokristallen und dem Polymer Poly(3-hexylthiophene-2,5-diyl) (P3HT) als Lochtransportschicht lieferte die höchsten Werte für die charakteristischen Parameter der Solarzellen.

Die Solarzellen wurden mittels UV/Vis Spektroskopie, Schichtdickenmessung, Fluoreszenzspektroskopie, Strom-Spannungskurven und der Messung der externen Quantenausbeute charakterisiert.

Acknowledgements

I would like to thank Assoc. Prof. Dipl.-Ing. Dr. techn. Gregor Trimmel for giving me the opportunity of writing my master thesis in his working group. Thank you for all your help during my work and for your supervision.

My deepest appreciation goes to Dr. Thomas Rath, who was like a co-supervisor for me, for the great support during my work, for the provided help for nearly every problem, for all ideas and expedient discussions.

I would like to thank all members of the Institute for Chemistry and Technology of Materials, especially those of my working group. Thank you for the warm atmosphere as well as for your great support and huge help in every situation. Moreover, I would like to offer my special thanks to my folks in the office, DI Bianca Wirnsberger, Bastian Friesenbichler and Benjamin Kain for the very enjoyable working atmosphere and for your unconditional support during the last months.

I owe a very important debt to Birgit Kunert for the XRD measurements, Amtsrätin Ing. Josefine Hobisch for the TGA analyses, DI Dr. Manuel Hollauf for the NMR measurements and DI Dr. Karin Wewerka and DI Dr. Ilse Letofsky-Papst for the TEM images.

I am deeply grateful to my girls Karin and Isabel, thank you for your unconditional friendship and all your support in our years of studying.

Finally, and most of all I would like to express the deepest appreciation to my family. Thank you for all your support in every possible and impossible situation during my whole life. Without your understanding and motivation in the last few years I would not be where I am now.

Content

1   Introduction

1.1   World energy consumption

The world's population and therefore the world energy demand has increased dramatically in the last 50 years (Figure 1).[1] The highest fraction of the energy consumption corresponds to the fraction of fossil derived energy. Since the available amounts of fossil fuels are not unlimited and not evenly distributed current and future sources of energy should be more sustainable. It is necessary that they are renewable and cause low carbon dioxide emissions.[2] Due to the increased consumption of fossil fuels also the carbon dioxide emissions strongly increased. If those emissions would not be reduced the global average temperature will increase.[3]
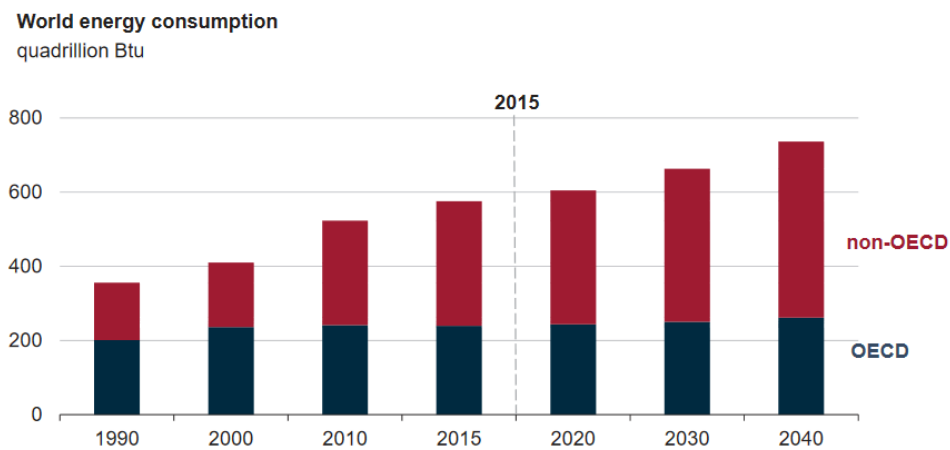

Figure 1: International energy consumption outlook 2017 (Source: U.S. Energy Information Administration (Sep 2017))[1]

Along with minimizing the consumption of fossil fuels the demand of renewable resources will rise (Figure 2).
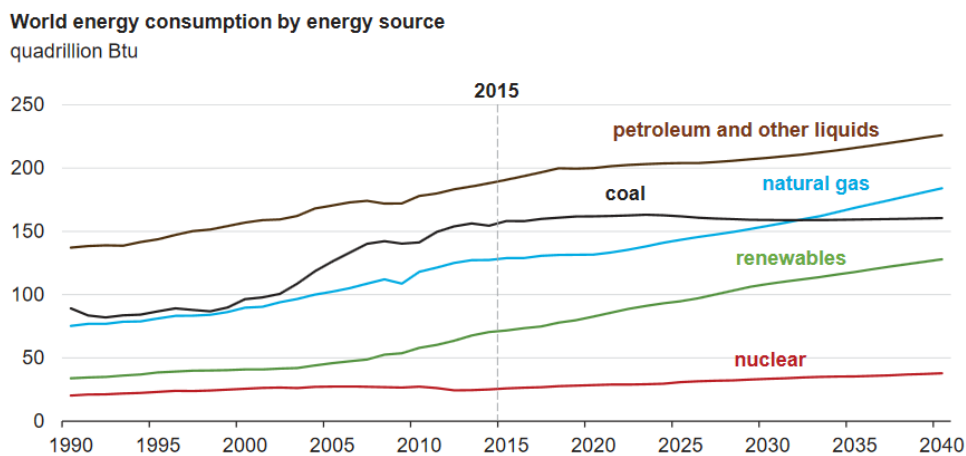

Figure 2: International energy consumption outlook by energy source 2017 (Source: U.S. Energy Information Administration (Sep 2017)) [1]

The most abundant source of energy on our planet is solar power. Low-cost, efficient solar cells would be a possibility to overcome the dependency on fossil fuels. Nowadays only 1.3% of the overall power used comes from solar power due to high costs compared to the use of fossil fuels. The promotion of research on the topic of photovoltaics would be a good investment in the future. Photovoltaics hardly create any carbon dioxide emissions when being used and are non-polluting, such as fossil fuels do and do not create any waste which nuclear energy does. Solar energy is therefore a true renewable resource.[4,5]

1.2 Aim of the Thesis

The aim of this thesis is to investigate synthesis routes of $CuInS_2$ nanocrystals by testing the heat-up method and the hot-injection method, respectively. Different copper and indium precursors, sulfur sources or molecular precursors (e.g. metal xanthates) and capping agents are used. The synthesized nanocrystals are characterized by X-ray diffraction measurement, transmission electron microscopy and UV/Vis spectroscopy.

The long-chained, insulating capping agents of the nanocrystals should be exchanged by shorter ligands. Afterwards, the ligand-exchanged nanocrystals should be incorporated into polymer/nanocrystal hybrid solar cells as well as quantum-dot sensitized solar cells.

The solar cells are characterized by UV/Vis spectroscopy, profilometer measurements, photoluminescence quenching experiments, current-voltage curves and external quantum efficiency.

The next chapters deal with the basics of solar cells and give an additional introduction into hybrid solar cells. Moreover, preparation methods for nanocrystals and for $CuInS_2$ nanocrystals in particular as well as possibilities for their modification are discussed.

In chapter 3 the results of the experimental work are displayed. This chapter is divided into three main parts. At first the research for an appropriate synthesis method is discussed, the following two parts consist of the main ligand exchanges, which were done in this thesis and the results of the solar cells, where the ligand-exchanged nanocrystals were incorporated.

The experimental work is described in detail chapter 4. Different preparation methods of the crystals, their ligand exchanges as well as the solar cell preparation are included.

A summary and an outlook are presented in chapter 5.

2   Theory

2.1   Basics of Solar Cells

Solid materials can be categorized depending on their electrical conductivity into three main groups, insulators, semiconductors and conductors. Energy bands are formed if individual atoms are arranged as crystal lattices like in solids. These bands indicate the allowed states of the energies of the electrons. Electrons in their lowest energy state stay in the so-called valence band and cannot move. The first non-occupied energy band is the conduction band. When the electrons in the valence band gain a discreet amount of energy they can move from the top of the valence band to the bottom of the conduction band. There they are free to move to other free energy states under the forces of an electric field or diffusion. The gained energy should be higher than the energy difference between the bands, which is called the band gap. The energy of the bandgap depends mainly on the composition and the temperature of the material.[6–8]

Coming back to the three main groups of conducting materials their properties can be explained with the mentioned model of energy bands. In a conducting material, the valence and the conducting band are overlapping, so electrons can move freely also at low temperatures and a band gap does not exist. Due to the overlapping, electrons of the valence band can move into the conduction band and so both are only partly filled and a high conductivity is given. Insulators have a fully filled valence band and a big gap between the bands which means that the difference is more than 3 eV. The valence electrons are tightly bound to the atoms and cannot move freely. So, the energy required for the electrons to overcome the energy barrier is also too high at high temperatures. Semiconductors are insulators at low temperatures. With a small amount of energy, as for example heat, the band gap of semiconductors is low enough that valence electrons can move into the conduction band. Figure 3 shows the energy bands of the three different types. [6–8]
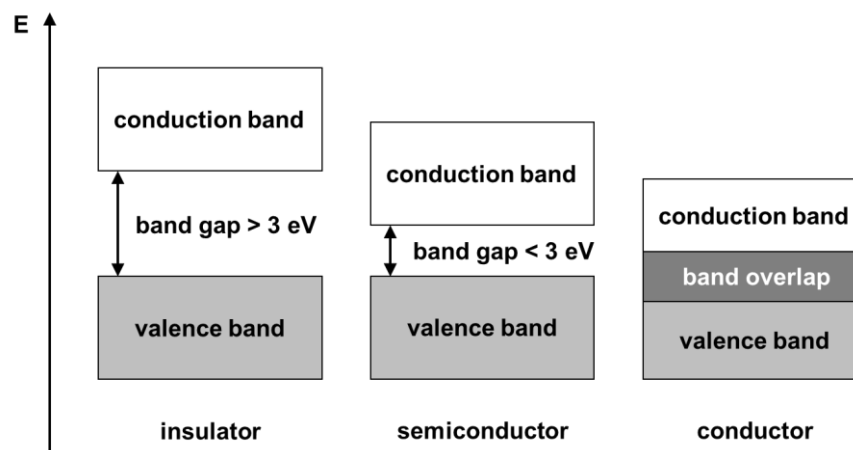

Figure 3: Energy band diagram of different types of materials

Examples for semiconductors are the elements silicon and germanium as well as compound semiconductors like GaAs, InAs and GaSb.[8]

The conductivity of the semiconductors can be improved by introducing impurities. For example, silicon has four valence electrons and is covalently bonded to four neighboring atoms. If one atom of phosphorous, which has five valence electrons, is introduced into the silicon lattice as a substitution for one silicon atom one electron is left unbound in the lattice. This additional electron is free for electrical conductivity already at room temperature. This type of substitution is called n-doping. A second possibility for changing the conductivity of a semiconductor is called p-doping. If one atom of boron, which has only three valence electrons, is introduced into the silicon lattice as a substitution for one silicon atom one electron is missing to complete covalence bonding. A hole and therefore hole conductivity is created. [6,7]

A p-doped and a n-doped semiconductor can be combined to a so-called p-n-junction. The n-doped region has an excess of electrons. These electrons move due to a concentration gradient to the p-doped side and recombine with the holes. Also, the holes move to the n-doped side and recombine with the electrons. Each electron and hole which leaves its "side" leaves a positively or negatively charged atom behind which acts as stationary charge. Due to the increasing number of stationary charges an electric field and therefore a field current in opposite direction is generated. The so-called space charge region is created.[7]

When a semiconductor is exposed to light and absorbs energy equal or higher than its band gap one photon makes one electron move from the valence band into the conduction band. An electron-hole pair is generated. Although the electron-hole pairs are held together by Coulomb forces, they are separated in the space charge region. The electrons move to the positive space charge region (n-region) and the holes move to the negative space charge region (p-region). A photocurrent, which is proportional to the incident light, is generated and can be measured.[6,7]

2.2 Hybrid solar cells

First generation solar cells are still dominating the market due to their high power conversion efficiencies around 21%.[9] A drawback of these crystalline silicon solar cells are the high costs for their manufacturing. The techniques for purification as well as the high temperatures lead to high energy costs. A lot of research for finding alternatives was done. Different concepts have been developed so far: polymer/nanocrystal solar cells, silicon-organic hybrid solar cells, dye-sensitized solar cells and organic-inorganic perovskite solar cells.[6] In inorganic thin film devices the costs can be decreased by reducing the thickness of the semiconducting layer. Due to the limited crystallinity of the thin film also the efficiency is lowered. A drawback of this devices is the use of rare materials. Examples for currently used compounds are $Cu(In, Ga)Se_2$

and CdTe. Organic solar cells have drawn the attention of research due to their low production costs, their ease in manufacturing and their high absorption coefficient. However, they have stability issues due to sensitivity to moisture and oxygen. The combination of organic materials, which are flexible, scalable and simple in manufacturing, with inorganic semiconductors, which have a high charge carrier mobility and high stability, led to the concept of hybrid solar cells.[10,11]

Polymer/nanocrystal solar cells are based on conjugated polymers and inorganic semiconducting nanocrystals. Due to the high absorption coefficient of the organic polymer also thin films are possible. Still enough solar energy is absorbed and due to a reduction in material the manufacturing costs are reduced. The inorganic nanocrystals can be tuned in their light absorption properties via shape and size due to quantum confinement, which provides the possibility of supplementing the missing part of the absorption spectrum.[10] Examples for investigated and used organic materials are conjugated polymers such as polythiophenes, PCDTBT, PTB7 and many more. Inorganic nanocrystals of CdSe, CdS, PbS, TiO_2, $CuIn_xGa_{(1-x)}Se_2$ and $CuInS_2$ and many more have been investigated.[10,12]

The first polymer/nanocrystal solar cell was published by Greenham in 1996. The cell consisted of CdSe nanocrystals and the polymer poly(2-methoxy-5-(2'-ethyl)-hexyloxy-phenylenevinylene) (MEH-PPV)[13]. Today, the highest power conversion efficiency reached is 5.5% by using the low band gap polymer PDTPBT in combination with PbS_xSe_{1-x} nanocrystals.[14]

2.2.1 Principle and device architecture of hybrid solar cells

In hybrid solar cells two different semiconductors work by the principle of a heterojunction solar cell where in most cases the organic polymer works as the donor and the inorganic nanocrystals work as the acceptor. Together they form the active layer because both materials can absorb light. Figure 4 describes the physical principle of a hybrid solar cell.[10,15]
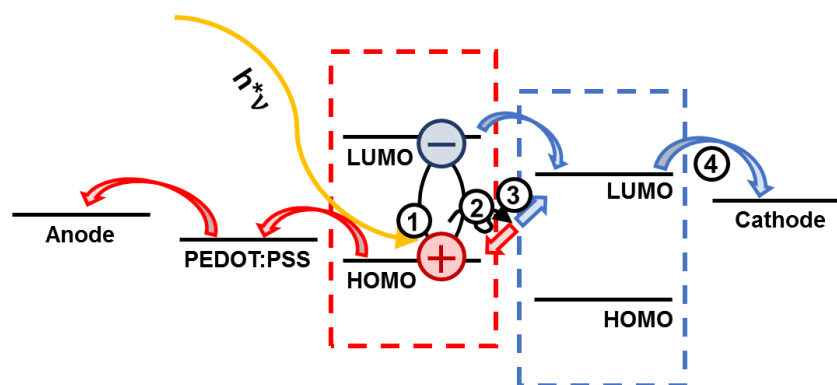

Figure 4: Physical principle of a hybrid solar cell: (1) photon absorption, (2) exciton diffusion, (3) charge separation, (4) charge transport

When the hybrid solar cell is exposed to solar energy and a photon with an energy at least as high as its bandgap energy is absorbed by the polymer, an electron is excited from the highest occupied molecular orbital (HOMO) to the lowest unoccupied molecular orbital (LUMO).

The excited electron has a reduced mobility because it is bound by Coulomb forces to the generated hole. This electron–hole pair is called exciton. When the exciton reaches the interface between the polymer and the nanocrystal, the electron and the hole are separated. The energy needed for separation is supplied by the difference of energy levels between the LUMOs of the polymer and the nanocrystal. The exciton dissociates into an electron and a hole, the hole remains in the HOMO of the polymer. The electron is transported through the nanocrystals to the cathode which has its energy level slightly below the LUMO of the nanocrystal. The holes move through the polymer to the anode after passing the electron-blocking but highly hole conductive PEDOT:PSS layer. The nanocrystals can also absorb photons. The holes are transferred in this case to the HOMO of the polymer and the electrons remain in the nanocrystal phase. The electrons and holes are, as already described, transported to the respective electrodes.[10,15]

The basic hybrid solar cell consists of the following layers. The anode of the solar cell consists of a thin transparent layer of indium tin oxide (ITO) coated on a glass slice or polymer foil like polyethylene terephthalate (PET). ITO is used because it has a wide bandgap and has a high light transmittivity in the visible range. On top of the ITO layer, generally a PEDOT:PSS layer is deposited which smoothes the ITO surface. The active layer, which consists as already described of the conjugated polymer and the nanocrystals, is deposited on top of the PEDOT:PSS layer. As last layer, a thin metallic electrode for electron collection is deposited. Usually aluminum or silver are used and deposited by thermal evaporation.[10,15]

There are two different structures of the active layer possible for the heterojunction solar cell. The first possibility is the creation of a bilayer between the organic polymer and the inorganic nanocrystals with a single heterojunction interface. Due to the existence of only one flat interface the area is smaller and the dissociation of the excitons is limited. The excitons can diffuse only for a short distance (~10 nm) in the polymer until they are recombined. To increase the area of the interface between polymer and nanocrystals a blend of the two compounds can be created. Due to a large dispersion of the interface area in the active layer, charge separation and transport are improved. More excitons can be dissociated and recombinations are less likely. This type is called bulk heterojunction (BHJ) and is the most commonly used structure for active layers. In Figure 5 the two types of device structures can be compared.[10,15]
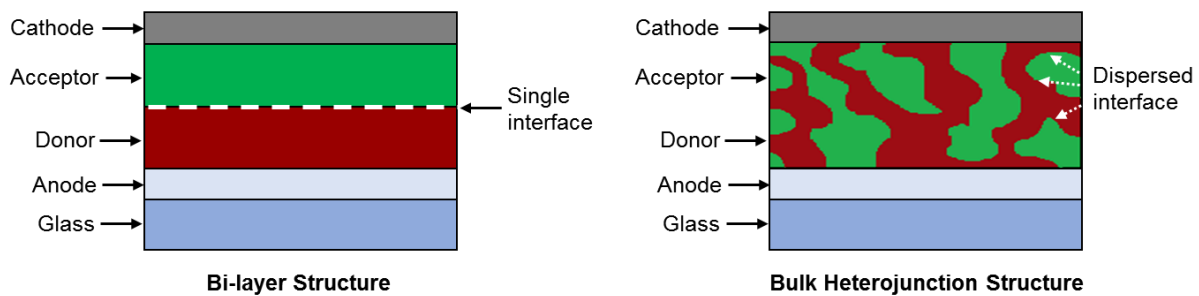
Figure 5: Sketches of a hybrid solar cell with a bilayer structure (left) and a bulk heterojunction structure (right)[10]

The LUMO level of the nanocrystals must be lower than the LUMO level of the polymer to guarantee the transfer of the electron. In addition, the HOMO level of the nanocrystals has to be lower than the HOMO level of the polymer to prevent the recombination of a hole with an electron. The band energy levels of the polymer and the nanocrystals should match for efficient charge separation and transfer at the interface. An optimum difference in energy gap of about 0.3 eV between the LUMO levels of polymer and nanocrystals was proposed. The energy difference between the LUMO level of the nanocrystals and the HOMO level of the polymer is proportional to the maximum possible open-circuit voltage (V_{oc}). A sketch of the energy levels of an ideal system of the polymer and the nanocrystals can be seen in Figure 6.[15]
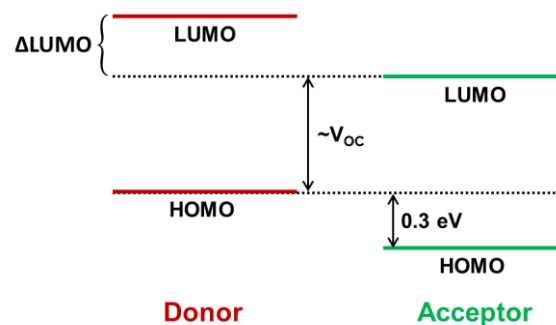
Figure 6: Sketch of the energy levels of an ideal system of materials for hybrid solar cell

2.2.2 Polymer/nanocrystal solar cell vs. quantum-dot-sensitized solar cell

As already mentioned in chapter 2.2 there are different approaches for hybrid solar cells in which organic and inorganic semiconducting materials are combined. Beside the classical solid-state devices, Grätzel et al. presented in 1991 the concept of a dye-sensitized solar cell as a low-cost and effective alternative for the first-generation solar cells.[16] In short, this kind of solar cell consists of a highly porous layer of n-type metal oxide such as TiO_2 onto a ITO-covered glass substrate which is coated with a monolayer of a photoactive dye. This light-harvesting complex is surrounded by a redox solution. Current is generated when the dye molecule is stimulated by incident photons, forms an excited state, and with good alignment of the energy levels of the compounds, charge separation of electron and hole occurs at the

interface of the metal oxide and the dye. Electrons are transported via the metal oxide to the electrode. The now oxidized dye is regenerated by the redox species in the liquid electrolyte.[17]

Although efficiencies up to 13%[18] are achieved nowadays, the approach with a liquid electrolyte included in a solar cell is not perfect. Evaporation of the solvent and its degradation as well as leakage of the electrolyte are several problems with which one has to deal with. These problems can be prevented by replacing the liquid electrolyte by a solid conductor. In a solid electrolyte there can be problems with the low mobility of the ions. Usually a p-type semiconductor, which is a good hole transport medium, is chosen.[18,19]

Not only the use of a liquid electrolyte but also the use of the dye is not that easy. A big drawback of a dye in a solid-state stack is that only with the adsorption of one monolayer of the dye onto the mesoporous metal oxide a good performance is achieved. So, a big surface area of the photoanode and a good charge transport across the crystals of the metal oxide are necessary. An increase of the thickness of the metal oxide layer would not deliver the desired increase in current. A lot of research was done to find materials as an exchange for the dye with a high absorption coefficient and efficient performance with more than one monolayer deposited. By exchanging the dye with for example inorganic absorber materials, the efficiency can be increased.[17]

An approach for exchanging the dye in solid-state devices is the usage of quantum dots. The materials used are usually inorganic semiconductors which have many interesting properties such as a high absorption coefficient, high intrinsic carrier mobilities and dipole moments. A big advantage is the opportunity of tuning their bandgap by simply changing their size or composition. In contrast to metal-organic dyes, inorganic semiconductors are also thermodynamically and optically stable. A drawback is the short life time of the charge carriers in the quantum-dot layer and the increase of recombinations of charge carriers if the thickness of the layer is increased. Examples are CdS, PbS, $CuInS_2$, $CuInSe$ etc.[17,20]

Comparing both types, polymer/nanocrystal solar cells and quantum-dot sensitized solar cells, there are more differences than only their different setup. Firstly, a mesoporous layer is required in the quantum-dot sensitized solar cell which is not needed in the polymer/nanocrystal solar cell. Additionally, in the quantum-dot sensitized solar cell the excitons are mainly generated at the nanocrystal and the polymer, which works only as hole transport layer, whereas in the polymer/nanocrystal solar cell the excitons can be generated on the interface of both materials and in the nanocrystal. In Figure 7 the two setups can be compared.
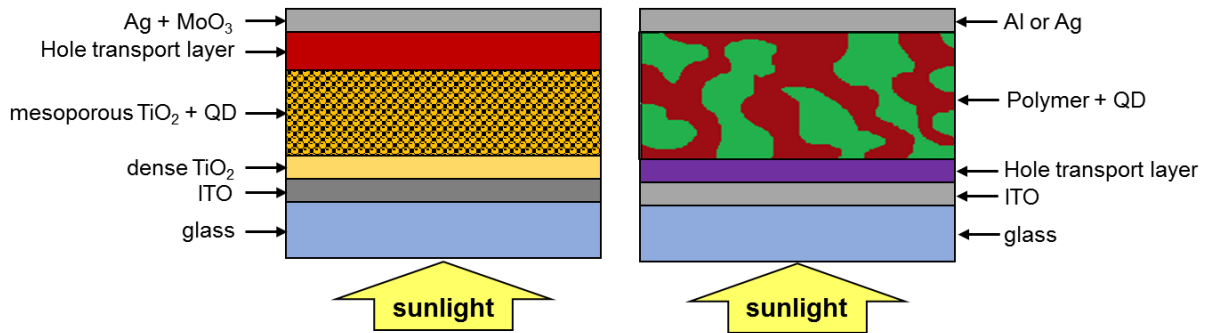
Figure 7: Sketches of quantum-dot sensitized solar cell (left) and nanocomposite solar cell (right)

The working principles for each type have already been explained above and in chapter 2.2.1.

2.3 Preparation routes of nanocomposite layers in hybrid solar cells

A lot of research was done not only on finding new combinations of materials for hybrid solar cells, but also on developing new preparation routes of such hybrid materials for the application in solar cells. The control of the synthetic process is very important because the efficiency of the solar cell is influenced by impurities in the active layer such as byproducts of the nanocrystal synthesis, capping agents and defects in or on the nanocrystals. The various synthetic routes can be roughly divided into three groups, the classical, the infiltration and the in situ approach.[5] A scheme of the three types is shown in Figure 8.
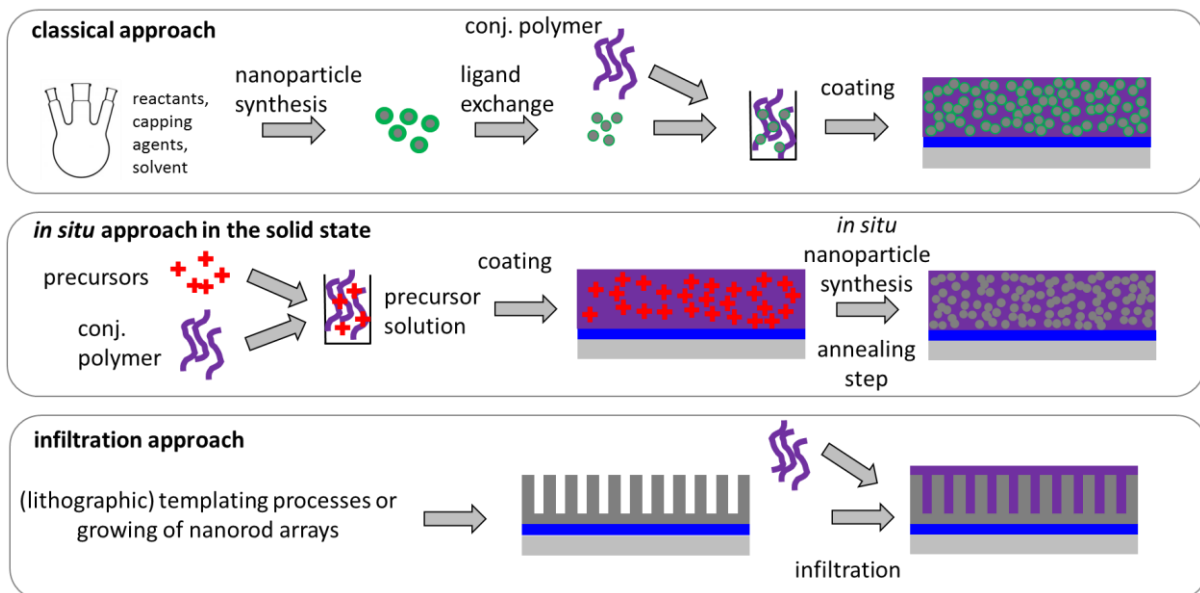
Figure 8: Preparation strategies of nanocomposite layers for hybrid solar cells (©Thomas Rath)

In the classical approach, which is the most frequently applied route, the nanocrystals are prepared via colloidal synthesis. Here the nanocrystals are synthesized in one pot via a hot-injection, heating-up or solvothermal method. In the hot-injection method the precursors are injected in a hot solution of the solvent(s) whereas in the heating-up method all components are heated up together and the nanocrystals formed in situ.[21] The synthesis of the particles is the first preparation step and is followed by purification and usually by a ligand exchange

process. In a last step the nanocrystals are dissolved together with the conjugated polymer forming the solution for the coating of the active layer. The capping agent, which stabilizes the nanocrystals, plays an important role concerning the appearance of the particles. It prevents the agglomeration of the particles and controls the size and the shape of the particles. A narrow distribution of size and an adjustment of shape and size of the particles is possible. A drawback of the usage of long-chained ligands, which are necessary to form the particles, is their effect of acting as a barrier for the charge dissociation and transport within the solar cell. Therefore, an exchange of the ligands with smaller ones is very important for achieving a good efficiency. Ligands like long-chained amines, phosphines or phosphine oxides are exchanged with shorter ligands like pyridine, small amines or thiols. Beside the positive effect on the electron transport and the charge distribution with shorter chain length, the solubility of the particles is reduced. This problem can be avoided by exchanging the ligands in the solid state after coating the solution of nanocrystals and polymer onto the substrate.[5,22]

In the infiltration approach inorganic nanostructures, which can be porous or mesoporous, are preformed on one electrode and filled with the organic polymer. Since the whole inorganic phase is already connected to the right electrode dead ends can be excluded. In this approach no ligands are needed for the formation of nanocrystals and therefore the problems which occur in the classical approach are avoided. Also, the formation of highly ordered structures is possible in this approach which is not achievable in the classical or the in situ approach. Beside those positive aspects there are also drawbacks. The preparation of the nanostructures needs complex steps in processing as well as high temperatures and long reaction times.[5]

In the in situ approach the nanocrystals are directly formed in the polymer matrix. A solution containing both, the organic polymer and the nanocrystal precursors is coated onto a substrate. In a thermal annealing step after the coating, the precursors are converted into the inorganic nanocrystals. Therefore, the biggest advantage of this approach is that no ligands are necessary for the formation of the particles. The polymer itself acts already as a capping agent and prevents an extensive growth of the particles. Due to the direct contact of the particles to the polymer and also between the nanocrystals themselves charge transport is facilitated. For the formation of the nanocrystals only moderate temperatures can be used. The optoelectronic properties and the structure of the conjugated polymer would be harmed by high temperatures. Due to a high viscosity of the polymer melt and the moderate temperatures, the crystal growth of the particles is strongly influenced and the appearance of the particles cannot be varied that easily as with the classical approach. This might cause a higher defect density and a lower crystallinity of the inorganic particles resulting in worse electronic properties.[5,22]

2.4 Copper Indium Disulfide

Copper indium disulfide (CIS), $CuInS_2$, is a direct semiconductor and an example for a ternary I−III−VI semiconductor. This material is a promising alternative for binary II-VI semiconductors like CdS or PbS. Cd and Pb are highly toxic and limit the II-VI semiconductors in their broad application range. $CuInS_2$ is less toxic and has similar optical properties as the above mentioned II-VI systems. CIS nanocrystals have a direct band gap (E_g = 1.5 eV) and a high absorption coefficient ($\alpha > 10^5\,cm^{-1}$) in the visible range.[23,24] The absorption and the emission can be tuned nearly over the whole visible region of the solar spectrum by changing the size of the particles. It was calculated by finite-depth-well effective mass approximation that the band gap of CIS nanocrystals with chalcopyrite structure, which is one possible structure, can be tuned between 3.3 and 1.7 eV with sizes between 1 and 6 nm. The band gap of the particles can also be influenced by the ratio of copper to indium. If the copper content is lowered, the band gap is increased.[23,24]

At room temperature, bulk copper indium disulfide has a chalcopyrite structure whereas the nanocrystals of this material can crystallize in three different structures (chalcopyrite, wurtzite, zinc blende). In this master thesis the chalcopyrite structure was preferred. Each sulfur atom is surrounded by two indium and copper atoms each. Due to differences in the bond lengths of Cu-S and In-S, anion displacement from a close-packed arrangement is caused. So, the crystal lattice has a tetragonal distortion.[23,24]

Due to the different chemical properties of the two cations Cu^+ and In^{3+} the synthesis of CIS nanocrystals is not that easy. Although the ionic radii of them are comparable (Cu^+ = 77 pm; In^{3+} = 80 pm) their bond lengths to sulfur and the reactivity toward sulfur compounds are different. In^{3+} is a hard and Cu^+ is a soft Lewis acid. Copper sulfide can be formed as a byproduct or completely instead of CIS if the precursors of the cations are not balanced.[23,24]

For the synthesis of CIS nanocrystals various approaches have been developed in the last few years using a variety of metal salts and sulfur sources. As solvent in most of the syntheses organic ones like oleic acid, oleylamine and octadecene are used. Beside various classical approaches for the growth of nanocrystals also in situ approaches have been developed. In the classical approaches sizes and shape of the particles can be controlled best with hot-injection or heating-up procedures. In this master thesis the focus was on the usage of metal xanthate precursors in a classical synthesis route.[5,23]

Metal xanthates react under elevated temperatures (below 200 °C) in an organic solvent via a Chugaev-like mechanism in which the xanthates decompose into volatile reaction products (alkene, OCS, SCS) and the respective metal sulfide nanocrystals (Figure 9).[25,26] Compared to other approaches for the synthesis of metal sulfide nanocrystals, xanthates have big

advantages. There is no external sulfur source necessary, because sulfur is already included in the xanthate structure itself. Additionally, in other approaches with metal salts also halides are included which are avoided within this approach.[23] Metal xanthates are easy in their usage and a good choice to minimize the development of disturbing byproducts.
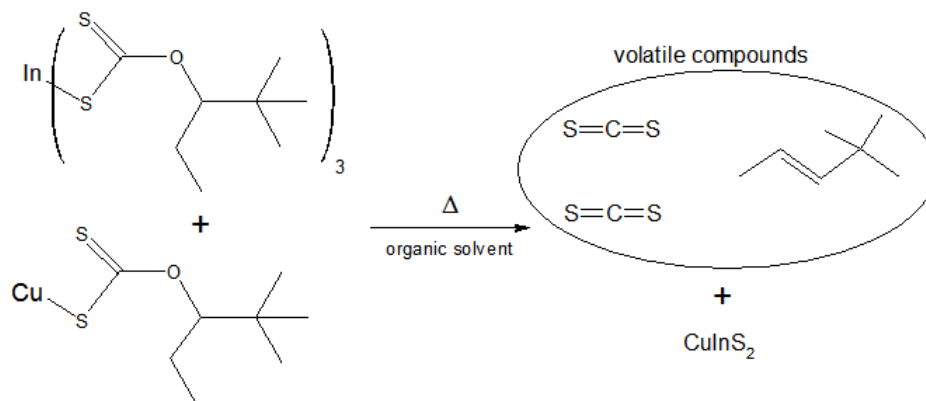

Figure 9: Reaction of copper and indium xanthates via heat to volatile compunds and CuInS₂ nanocrystals [26]

Due to their great properties mentioned above, CIS nanocrystals provide all requirements for the application in a hybrid solar cell. Arici et al. were the first who investigated the use of CIS in solar cells in 2003.[27] Thereafter much research was done on this topic.[26,28–31]

2.5 Ligand exchange of nanocrystals

There are several methods how nanocrystals are prepared for their use in hybrid solar cells as already explained in chapter 2.3. In this thesis the classical approach was in the focus of interest. Long-chained organic solvents are necessary in this approach to form the particles. A drawback of their usage is their negative effect on the charge dissociation at the interface between polymer and nanocrystal and the electron mobility through the nanocrystal phase as already explained above. A complete removal of the ligand shell is very difficult and would also lead to solubility problems and aggregation of the nanocrystals. For the collection of high photocurrent and therefore achieving a good efficiency of the solar cell an exchange of the long-chained ligands with shorter ones is very important.[5,10]

There are in principle two different methods for post-synthetic ligand exchange, colloidal ligand exchange or an exchange in the solid phase after layer deposition.[32]

In the approach of ligand exchange in the solid phase, the nanocrystals are first dispersed in a solvent, applied onto the desired substrate and the coated layer is afterwards treated with a solution of the new ligand. It was shown that this method is very effective, but due to the decreased volume of the ligand shell, cracks and void spaces are a negative side effect. These defects should be backfilled with additional nanocrystals.[32]

The ligand exchange in solution is carried out by addition of the new ligand to a dispersion of nanocrystals with the ligand which should be exchanged. Afterwards, a suitable antisolvent is added for assisting the removal of the former long-chained ligands. The addition of the antisolvent may be repeated several times to increase the effectiveness of the exchange of the ligands.[33] The ligand exchange done in solution increases the probability of direct formation of dense solids with short distance between the particles with no defects like cracks or void spaces.[32] The ligand exchange in solution was the method which was used in this thesis.

Very common is the exchange of the former ligand with pyridine due to its conjugated system and therefore good conductivity. Also, the ligand exchange with short alkyl thiols like *tert*-butylthiol or 1-hexanethiol is widely used.[5,10] In this thesis also a very simple ligand exchange with ammonium thiocyanate was investigated.[32]

A new approach of ligand exchanges is the use of "smart" ligands whose chains can be partly removed by heat or include conjugated systems in side groups of the polymer chain for improved charge dissociation and transport. A drawback of conjugated capping agents is the labor-intensive synthesis.[5]

Beside the methods of directly exchanging the ligands of the nanocrystals a simple strategy to remove the excess ligand by a washing treatment using hexanoic acid was introduced by Zhou et al.[34] There the former ligand (hexadecylamine) forms a salt with the acid which is easily dissolved in the solvent and so the ligand shell is reduced.

3   Results and Discussion

3.1   Synthesis of CIS nanocrystals

Several different classical approaches for the synthesis of copper indium disulfide nanocrystals as well as different exchanges of their ligands for further improvement for their use in solar cells were investigated. A chalcopyrite crystal structure of the nanocrystals is preferred.

First, CIS nanocrystals were synthesized using a modification of the method published by Kolny-Olesiak et al.[30], using copper acetate (CuAc) and indium acetate (In(Ac)$_3$) as precursors with a molar ratio of 1:1.7, oleylamine and octadecene as solvent and a mixture of *tert*-dodecanethiol and 1-dodecanethiol as capping agent and sulfur source. The molar ratio of 1:1.7 was used instead of 1:1 due to better results achieved in the research group.[22,26,35] The synthesis yielded CIS nanocrystals which can be seen in the following XRD pattern (Figure 10). By comparing the XRD pattern with the reference patterns for the wurtzite and the chalcopyrite structure it can be derived that the synthesized CIS nanocrystals do not have the desired chalcopyrite structure.
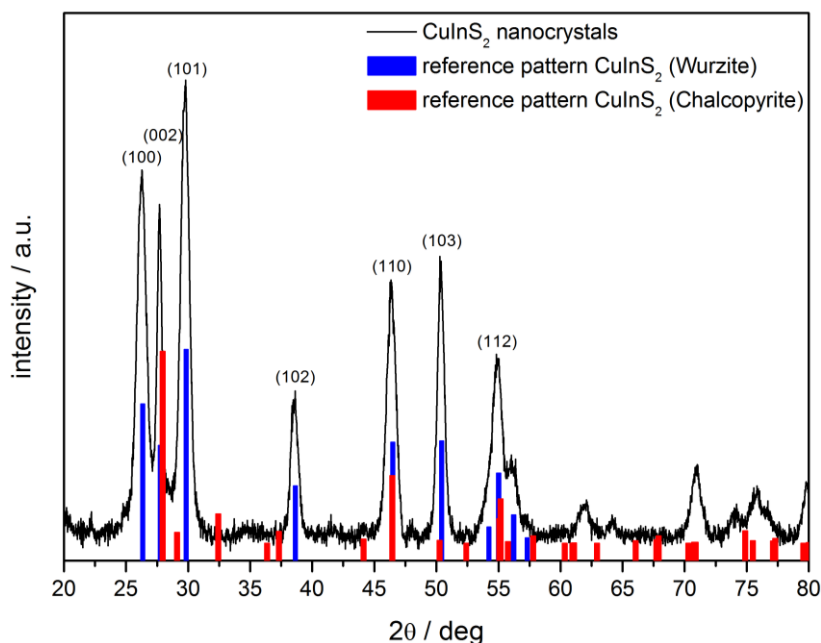

Figure 10: XRD pattern of CIS nanocrystals synthesized according to the method described in chapter 4.1.1

The CIS nanocrystals have a mixed crystal structure of wurtzite and chalcopyrite structure. The main peaks for the wurtzite structure are at 26.2° (100), 29.8° (101) and 38.6 (102). For the chalcopyrite structure the main peaks are at 27.9° (112), 46.5° (220) and 55.1° ((116) and (312)).

The size of the particles was estimated from the XRD pattern with the Scherrer equation:

$$D = \frac{K * \lambda}{(\Delta(2\theta) - x) * \cos(\theta)} \qquad (1)$$

D …….. particle diameter

K …….. shape factor; 0.9 for spherical particles

λ ……... wavelength

2θ ……. scattering angle

∆(2θ) … full width at half maximum of reflection in radians

θ ………half of scattering angle 2θ

x ……... correction for instrument broadening (0.12 2θ)

The calculated diameter for the particles with wurtzite structure was between 12.5 and 16.9 nm, for the particles with chalcopyrite structure between 13.8 and 19.3 nm

In a second attempt it was considered to use metal xanthates. The use of copper and indium xanthates provides an easy method to synthesize sulfide nanocrystals and volatile byproducts. *Tert*-dodecanethiol and 1-dodecanethiol, which were used as capping agent and sulfur source in the previous synthesis method, could not be further used due to the additional sulfur. So, it was searched for appropriate capping agents which could also be used as solvent. Oleylamine is already a favoured solvent in the synthesis of CIS nanocrystals. But also, a mixture of oleylamine with oleic acid is quite common.[23,36–38] It was decided to use a mixture of oleylamine and oleic acid with a ratio of 1:1. Due to the insolubility of the metal xanthates in oleylamine and oleic acid an additional solvent had to be found. Out of tested solvents with high boiling points (tetradecane and 1,2,4-Trichlorobenzene), 1,2,4-trichlorobenzene worked quite good.

In short, oleylamine and oleic acid were heated to 200 °C and copper O-2,2-dimethylpentan-3-yl dithiocarbonate and indium O-2,2-dimethylpentan-3-yl dithiocarbonate (1:1.7) dissolved in 1,2,4-trichlorobenzene were injected into the hot solution of capping agents.

The synthesis yielded copper indium disulfide nanocrystals which can be seen in the following XRD pattern (Figure 11). By comparing the reference patterns, it can be concluded that the nanocrystals had a chalcopyrite structure.
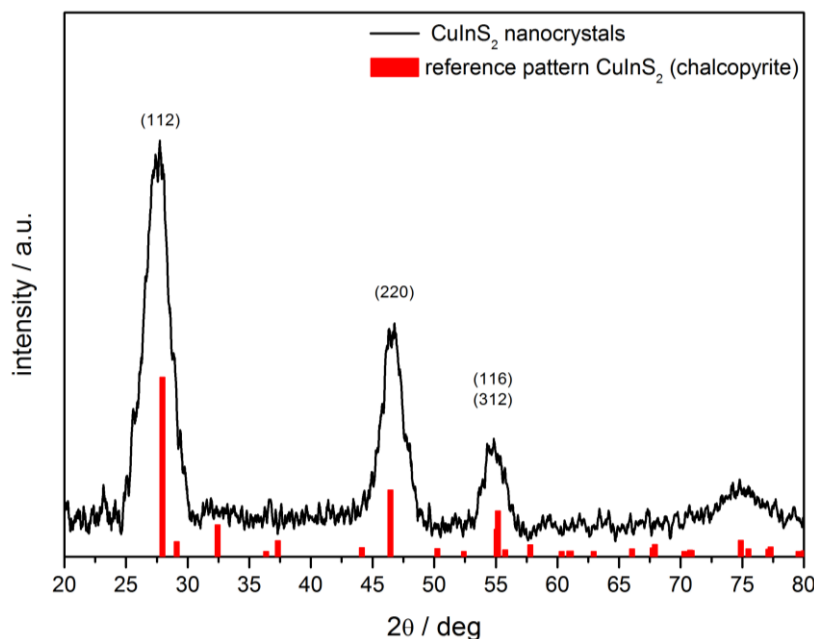
Figure 11: XRD pattern of CIS nanocrystals synthesized according to the method described in chapter 4.1.4

The three main peaks are at 28° (112), 46° (220) and 55° ((116) and (312)). The size of the particles was also estimated from the XRD pattern with the Scherrer equation (Equation 1). The calculated diameter for the particles was between 3.4 and 4.0 nm. Despite the small size further experiments were done with the nanocrystals synthesized with the metal xanthates as precursor.

In the following chapter the results of the analyses of CIS nanocrystals derived from the synthesis with the metal xanthates are presented. Afterwards, the results of the exchange of the ligands with 1-hexanethiol and ammonium thiocyanate as well as of the incorporation of the CIS nanocrystals in polymer/nanocrystal solar cells and quantum-dot sensitized solar cells are listed.

3.1.1 Transmission Electron Microscopy

For further analysis of the synthesized nanocrystals, they were investigated by transmission electron microscopy. Two images with different magnification can be seen in Figure 12. The diameter of the nanocrystals is between 4 and 6 nm which is comparable to the estimation from the XRD pattern with the Scherrer equation. A reason for the slight difference can be the difference between the two analysis methods. The XRD only shows the crystalline part of the particles whereas the TEM shows both, the crystalline and amorphous part.
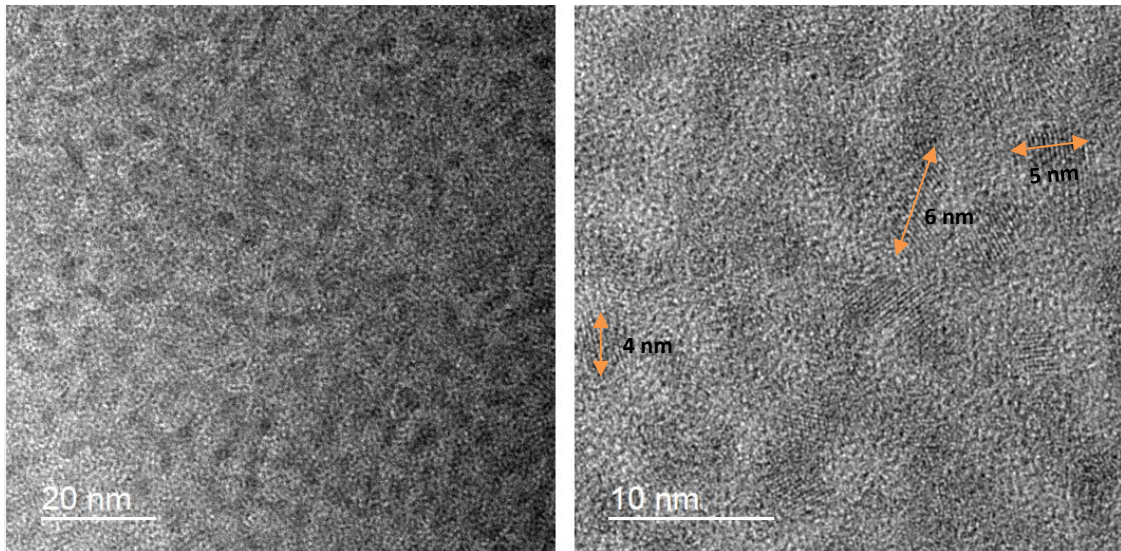
Figure 12: TEM images of CIS nanocrystals with dioleamide as capping agent

3.1.2 Determination of the band gap

Before the incorporation of the CIS nanocrystals into the setup of a polymer/nanocrystal hybrid solar cell, the band gap of the synthesized non-ligand exchanged particles was determined via the Tauc plot.

First an absorbance measurement of the CIS particles was done, afterwards the thickness of the prepared layer was determined by using a surface profiler. Both methods are described in detail in chapters 4.4.2 and 4.4.7.

Due to the huge amount of capping agent in the layer compared to the amount of pure CIS, which is the material of interest, the measured thickness of the layer does not represent the real thickness of the CIS layer. So, the measured layer thickness was reduced by the mass share of the capping agent over the mass change in the TGA and its density. For further calculation the thickness or the layer was decreased to around 7 µm instead of around 26 µm.

By combining the absorbance and the layer thickness the absorption coefficient which is needed for the determination of the optical band gap can be calculated with Equation 2.

$$\alpha = \frac{1}{d} * lnA \qquad\qquad \textbf{(2)}$$

d … layer thickness

A … Absorbance

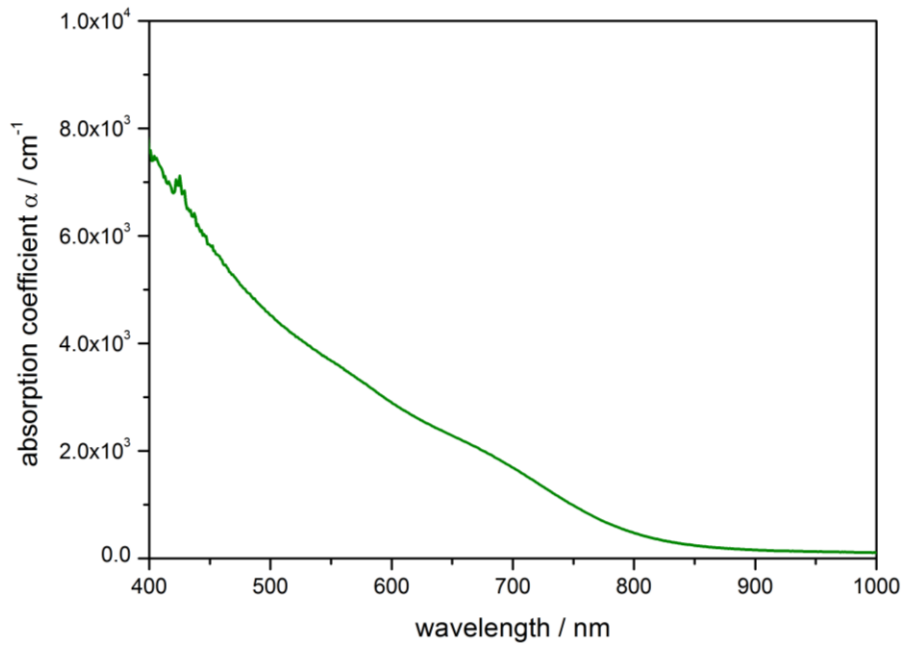The absorption profile is shown in Figure 13

Figure 13: Absorption profile of synthesized CIS nanocrystals

By combining the absorption coefficient and the photon energy, the optical band gap E_g can be received via Equation 3.

$$\alpha = \frac{C(h\nu * E_g)^n}{h\nu} \qquad (3)$$

C ..... constant

$h\nu$ … photon energy

n ..... exponent (here ½, due to direct band gap)[39]

By plotting $(\alpha h\nu)^2$ versus $h\nu$ the value for the band gap can be determined by linear extrapolation of the curve (Tauc plot).[40]
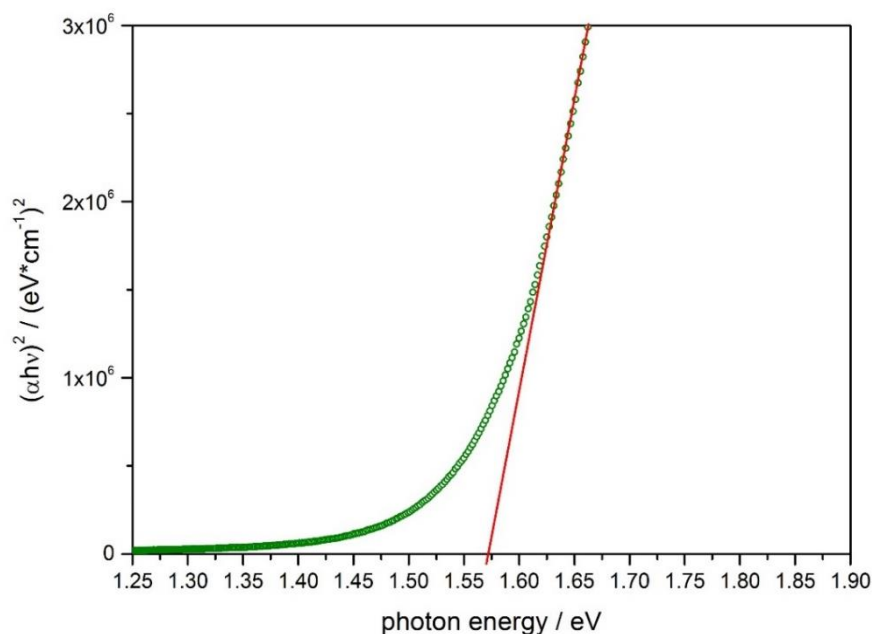
Figure 14: Determination of optical band gap of CuInS$_2$

The obtained band gap of around 1.57 eV is in the range of the values in literature.[41–43]

3.1.3 Analysis of capping agents

Due to a change in color of the solution of oleyl amine and oleic acid during heating in the synthesis method with the metal xanthates a NMR analysis was done. The two capping agents turned out to react to one single molecule when heated together beforehand, forming the new capping agent: dioleamide.[44] In Figure 15 the reaction mechanism and in Figure 16 the NMR pattern is shown.
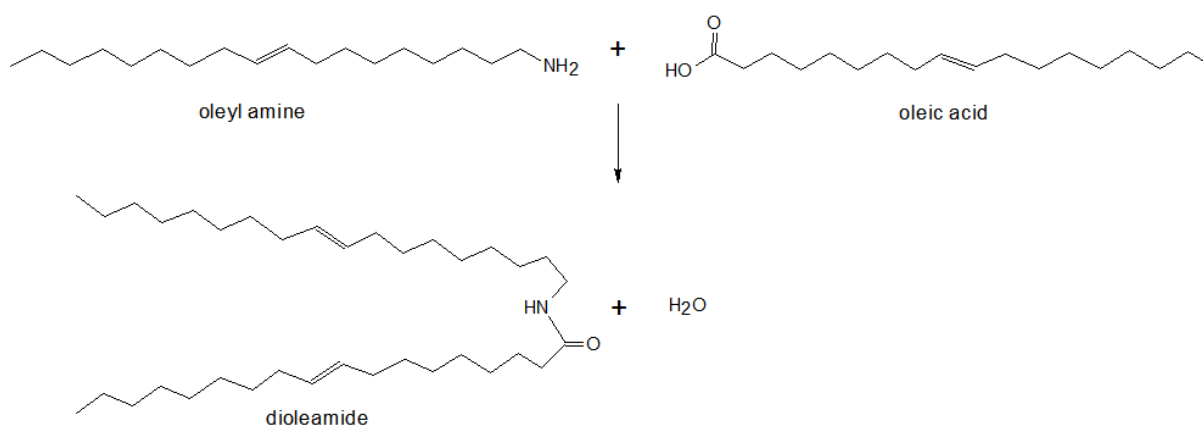

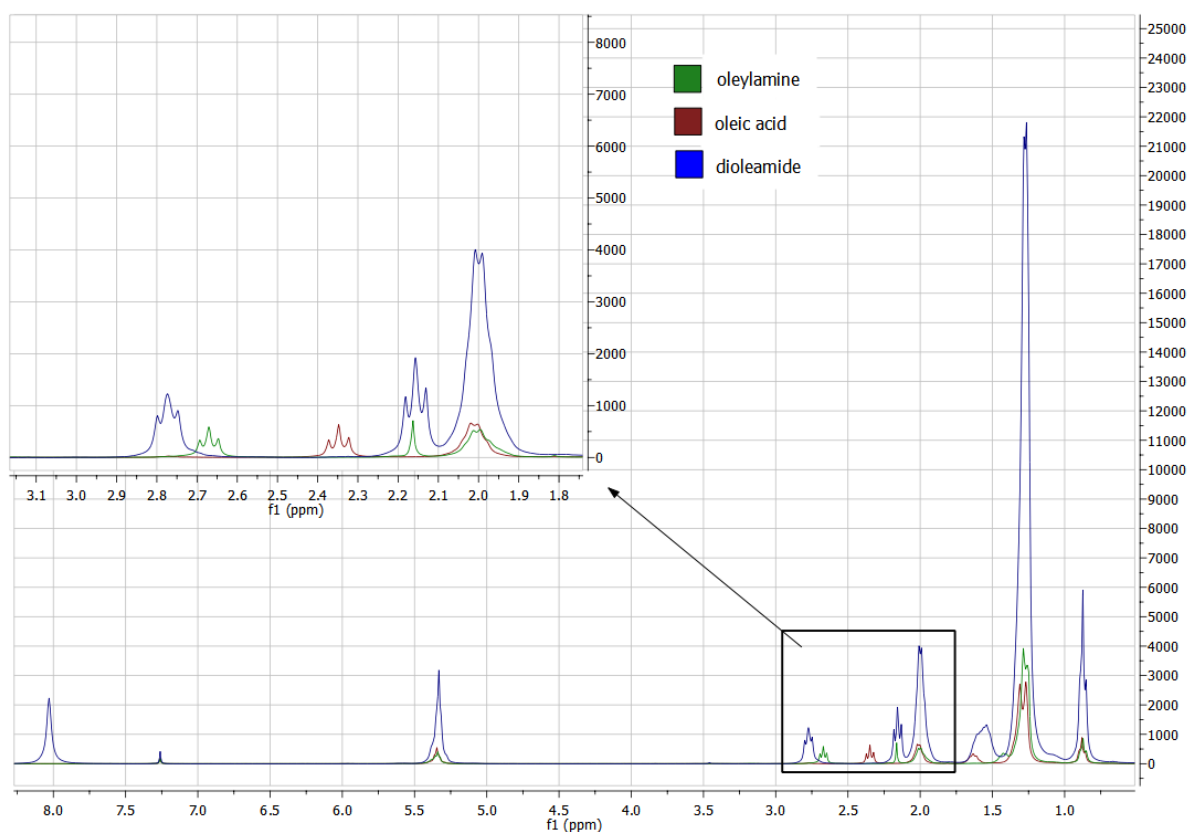**Figure 15: Reaction of oleyl amine and oleic acid to dioleamide[44]**

Figure 16: NMR pattern of oleyl amine, oleic acid and dioleamide

In the NMR pattern it can be distinguished between the educts oleyl amine and oleic acid and the product dioleamide. Despite the similarity in structure of the three molecules there are also some specific differences. Especially the area between 2.3 and 3.0 ppm is interesting (see detail). There are three triplets which are very different for each of the molecules. The triplet from oleic acid at 2.35 ppm belongs to the two hydrogen atoms beside the acid group, the one from oleyl amine at around 2.65 ppm belongs to the two hydrogen atoms beside the amine and the triplet from dioleamide at around 2.8 ppm belongs to the two hydrogens beside the nitrogen of the amide group. So, the existence of a different capping agent as expected was proofed.

3.2 Ligand exchange of nanocrystals

Due to the insulating properties of the long-chained capping agents, experiments were done to exchange them with shorter ligands. 1-Hexanethiol, ammonium thiocyanate, pyridine and 1,3-benzenedithiol were investigated for their suitability as new ligand. The pyridine-capped CIS nanocrystals did not dissolve in the desired solvent chlorobenzene. The ligand exchange with 1,3-benzenedithiol did not work at all. So, the methods using 1-hexanethiol and ammonium thiocyanate were optimized and analyzed further.

The ligand exchanges with 1-hexanethiol and ammonium thiocyanate were chosen due to the good solubility of the particles after exchange in chlorobenzene and dimethylformamide,

respectively. Additionally, the exchange of the former ligands with the new ones as well as the incorporation of the ligand-exchanged nanocrystals in the hybrid solar cell setups itself worked out best with these two methods.

3.2.1 Ligand exchange with 1-hexanethiol

3.2.1.1 FTIR spectroscopy

To confirm if the ligand exchange has worked properly, FTIR-spectroscopy was performed. Here only the ligand shell is characterized. The results of the analysis are shown in Figure 17.
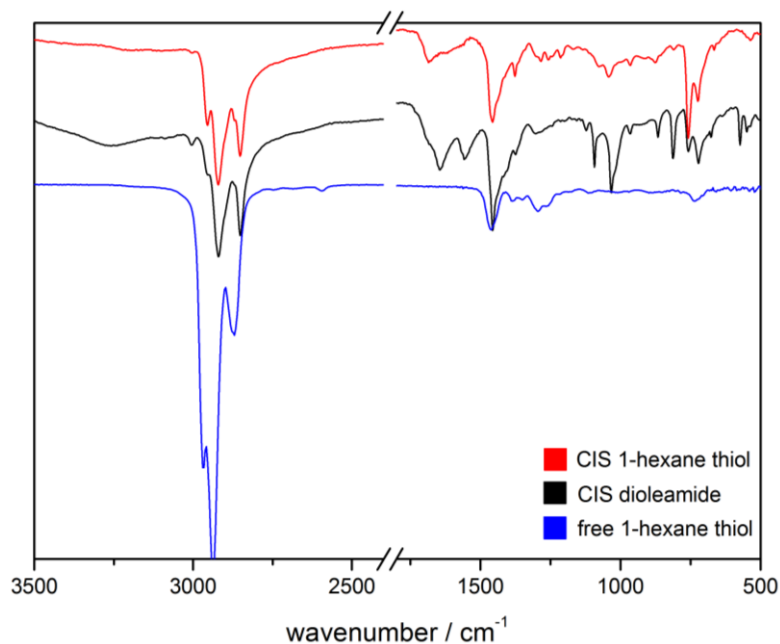

Figure 17: IR spectra of dioleamide and 1-hexanethiol in their corresponding CIS sample

The difference between the ligands dioleamide and 1-hexanethiol is not that easy to distinguish due to the alkyl chain present in both substances. In the spectrum of the non-ligand exchanged CIS nanocrystals there are two bands at 1558 and 1644 cm^{-1}, which correspond to the bending vibration of the N-H bond and to the stretching vibration of the C=O bond, respectively. The band at 1644 cm^{-1} also corresponds to the bending vibration of the C=C bonds. Additionally, there are two bands at 3005 cm^{-1}, which corresponds to the bending vibration of C-H at the C=C bond and at around 3260 cm^{-1}, which corresponds to the stretching vibration of the N-H. All these three bands which can be attributed to dioleamide are not present in the spectra of the ligand-exchanged CIS. The bands at 1458, 2852, 2921 and 2954 cm^{-1} are present in both samples of CIS and correspond to the scissor vibration of the C-H-bond, the asymmetric and symmetric stretching vibration of the C-H bond.

The unique band for 1-hexanethiol at 2594 cm^{-1}, which corresponds to the stretching vibration of the S-H bond, has only weak intensity. This may not be present in the spectra of the ligand-exchanged CIS due to a possible direct bond of sulfur onto the nanocrystals. The assignment of the FTIR results of the three samples is based on literature and summarized in Table 1.[45]

Table 1: assignment of IR bands of 1-hexanethiol and dioleamide adsorbed on CIS[45]

free 1-hexanethiol	
wave number [cm^{-1}]	**vibrations**
1458	scissor vib. (C-H) in R_2-CH_2
2594	v(S-H)
2870	v_{as}(C-H)
2938	v_s(C-H)
2970	v_s(C-H)
dioleamide adsorbed on CIS	
1458	scissor vib. (C-H) in R_2-CH_2
1558	δ(N-H)
1644	δ(-C=C) + v(C=O)
2852	v_{as}(C-H)
2921	v_s(C-H)
2954	v_s(C-H)
3005	δ(=C-H)
3260	v(N-H)
1-hexanethiol adsorbed on CIS	
1456	scissor vib. (C-H) in R_2-CH_2
2852	v_{as}(C-H)
2921	v_s(C-H)
2954	v_s(C-H)

3.2.1.2   Thermogravimetric analysis

For determination of the amount of capping agent adsorbed onto the CIS nanocrystals a thermogravimetric analysis was done. Also, the success of the ligand exchange can be investigated. Two measurements of the nanocrystals were done, before and after the ligand exchange (Figure 18).
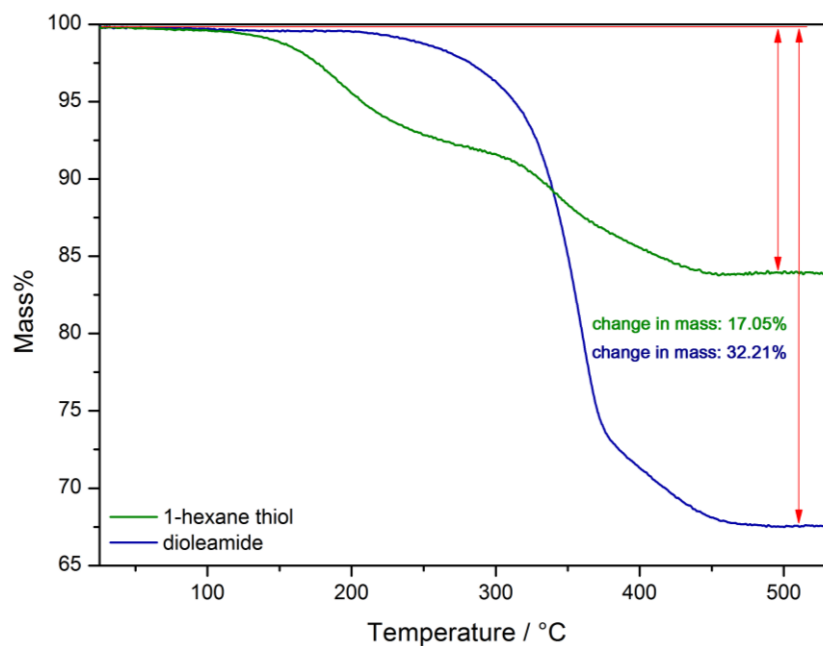
Figure 18: TGA curve of CIS nanocrystals before and after ligand exchange with 1-hexanethiol

The measured mass loss refers to the amount of the capping agents on the nanocrystals. The mass loss between 150 and 300°C in the sample of 1-hexanethiol capped CIS can be ascribed to free or loosely bound 1-hexanethiol still present in the sample after the precipitation step. Further mass loss above 300°C in both samples can be explained by the decomposition of dioleamide and 1-hexanethiol which are coordinated on the CIS nanocrystals, respectively. The difference in their mass loss is due to the much lower mass of 1-hexanethiol compared to dioleamide. But due to their smaller head group more 1-hexanethiol than dioleamide molecules can coordinate on the nanocrystal surface.

3.2.1.3 Transmission Electron Microscopy

To investigate changes in size and agglomeration behavior the 1-hexanthiol capped CIS nanocrystals were also analyzed by transmission electron microscopy. Two images with different magnification can be seen in Figure 19. The diameter of the nanocrystals is between 3 and 5 nm which is comparable to the of the dioleamide capped CIS crystals estimated on the TEM images. By comparing the images in Figure 12 and 19 the particles with the longer dioleamide ligand are arranged in a more ordered fashion whereas the particles with the shorter 1-hexanethiol ligand tend to agglomerate.
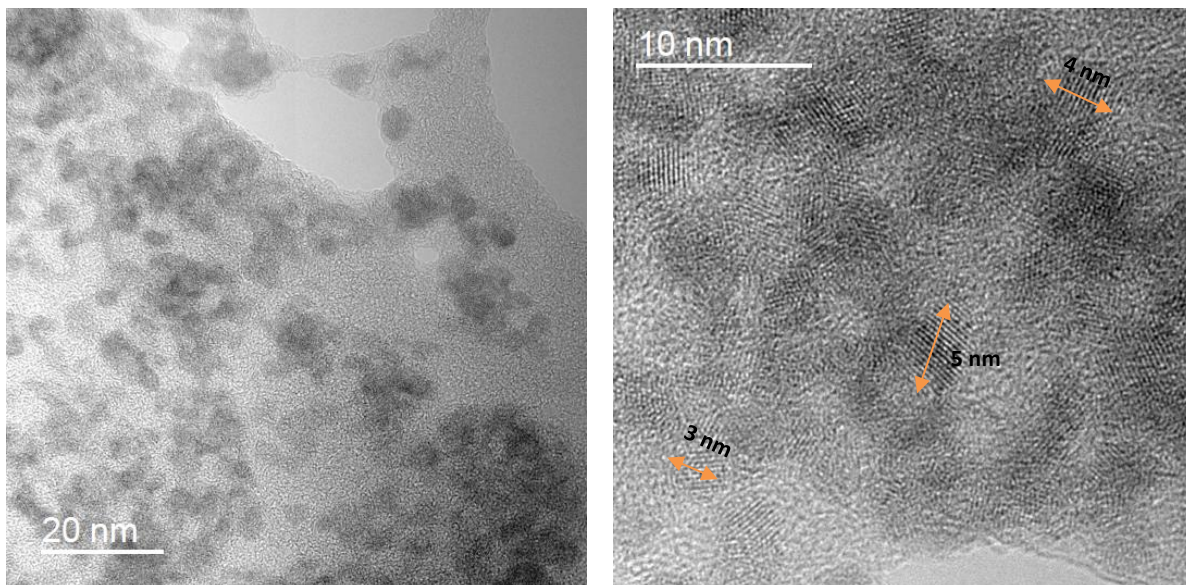
Figure 19: TEM images of CIS nanocrystals with 1-hexanethiol as capping agent

3.2.1.4 Incorporation of nanocrystals in hybrid solar cell

The aim of the incorporation of the CIS nanocrystals in hybrid solar cells was to test their functionality and applicability. Various ratios of polymer to CIS nanocrystals were investigated and the influence of annealing on the overall performance was tested. The overall results of the optimization of the devices is shown below. The presented results of open circuit voltage (V_{OC}), short circuit current (I_{SC}), fill factor (FF) and power conversion efficiency (PCE) are the average of the five best cells if not stated differently.

Solar cells with the bulk heterojunction assembly were built. The CIS nanocrystals acted as acceptor material and the conjugated polymer poly[N-9'-heptadecanyl-2,7-carbazole-alt-5,5-(4',7'-di-2-thienyl-2',1',3'-benzothiadiazole)] (PCDTBT) was used as donor material. Due to wettability problems using the dioleamide-capped CIS nanocrystals and therefore the impossibility of generating a uniform film on PEDOT:PSS, only the 1-hexanethiol capped CIS nanocrystals were used for further experiments.

3.2.1.4.1 Absorption measurement of active layer

For the determination of the absorption properties of the active layer, UV/Vis measurements were done as described in chapter 4.4.2. In Figure 20 the absorption spectra of the active layer with different ratios of polymer to CIS nanocrystals are shown.
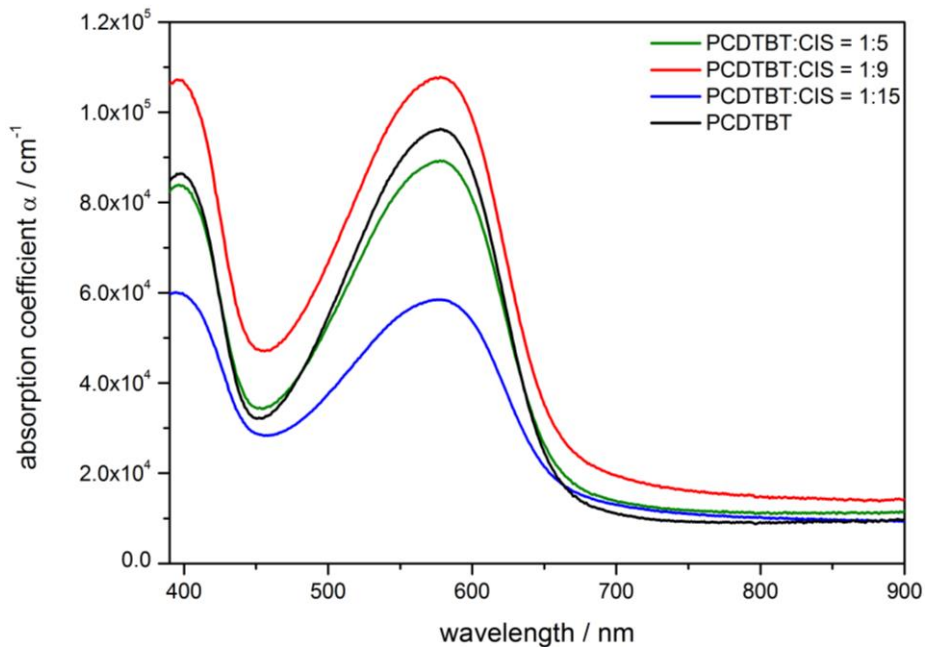
Figure 20: Optical absorption coefficient of active layers with different ratios of polymer to CIS nanocrystals

By comparing the pure PCDTBT with the samples of increasing CIS content the absorption coefficient does not increase with the amount of nanocrystals. Surprisingly, the layer with the highest amount of nanocrystals has the lowest absorption coefficient. The layer of pure PCDTBT and the one with the lowest amount of nanocrystals are comparable in their absorbance. At lower wavelength the differences in absorption of the samples are higher and decrease with increasing wavelength. PCDTBT has its absorption maxima at 397 and 578 nm and hardly absorbs after 700 nm.

3.2.1.4.2 PL Quenching Experiments

The performance in a polymer/nanocrystal hybrid solar cell strongly depends on the charge transfer between the polymer and the nanocrystal phase. Charge separation occurs at the interface of the two materials and the electron is transported to the nanocrystal. At the same time radiative decay to the ground state is impossible. So, the photoluminescence of the polymer is quenched if charge transfer occurs.[13]

The PL quenching experiments were conducted as described in chapter 4.4.8. Figure 21 shows the PL spectra of the active layer with different ratios of polymer to CIS nanocrystals with exchanged ligand. The PL intensities were normalized with the respective absorption coefficients. A decrease in photoluminescence with increasing content of CIS nanocrystals can be detected. The charge transfer from the polymer to the nanocrystals works as expected.
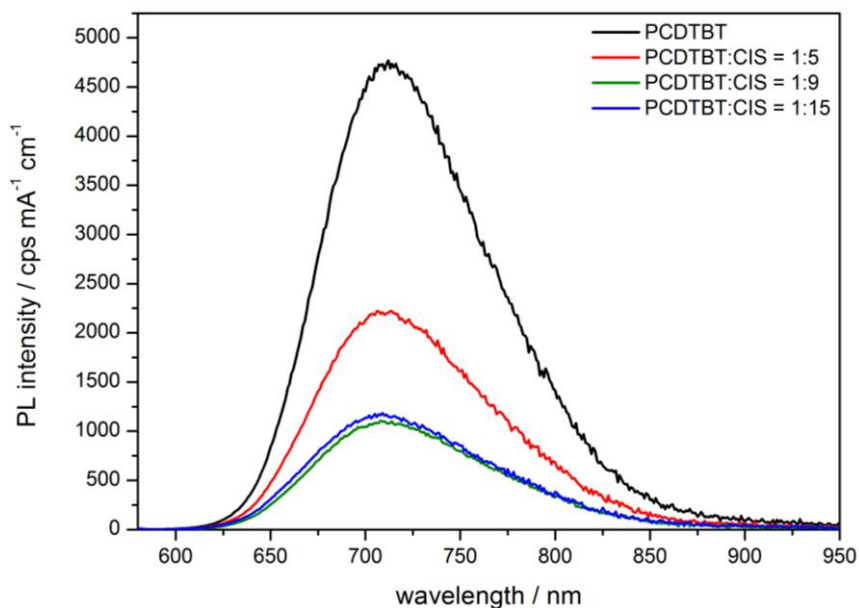
Figure 21:PL spectra of active layers with different ratios of polymer to CIS nanocrystals with exchanged ligand

For comparison, the PL spectra of the active layer with different ratios of polymer to CIS nanocrystals with the dioleamide ligand are shown in Figure 22.
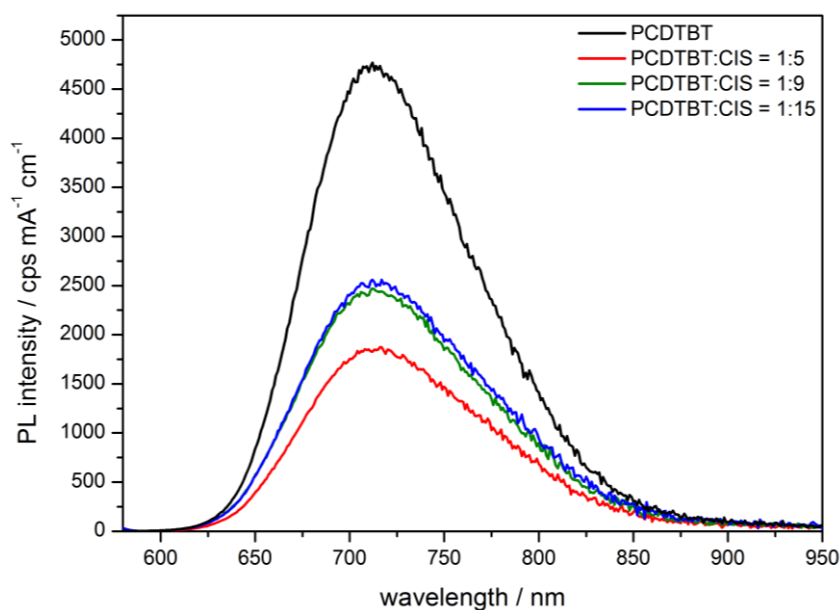

Figure 22:PL spectra of active layers with different ratios of polymer to CIS nanocrystals with dioleamide ligand

Surprisingly, the charge transfer between the polymer and the CIS particles, where no ligand exchange was done, worked out quite well and the photoluminescence of the polymer was quenched. This happens due to the good distribution of the particles in the polymer. But with increasing CIS content it can be detected that the photoluminescence is worse than with low CIS content. Further charge transfer and therefore quenching with increasing amount of dioleamide-capped nanocrystals is hindered by the long-chained ligands. The photoluminescence of the polymer was also quenched very good by the 1-hexanethiol capped CIS nanocrystals.

3.2.1.4.3 Atomic Force Microscopy

For visualization of the distribution of the CIS nanocrystals in the polymer and the surface structure of the solar cell, atomic force microscopy was done of the solar cell with the highest efficiency. In Figure 23 the topography (left) and the phase image (right) are shown.
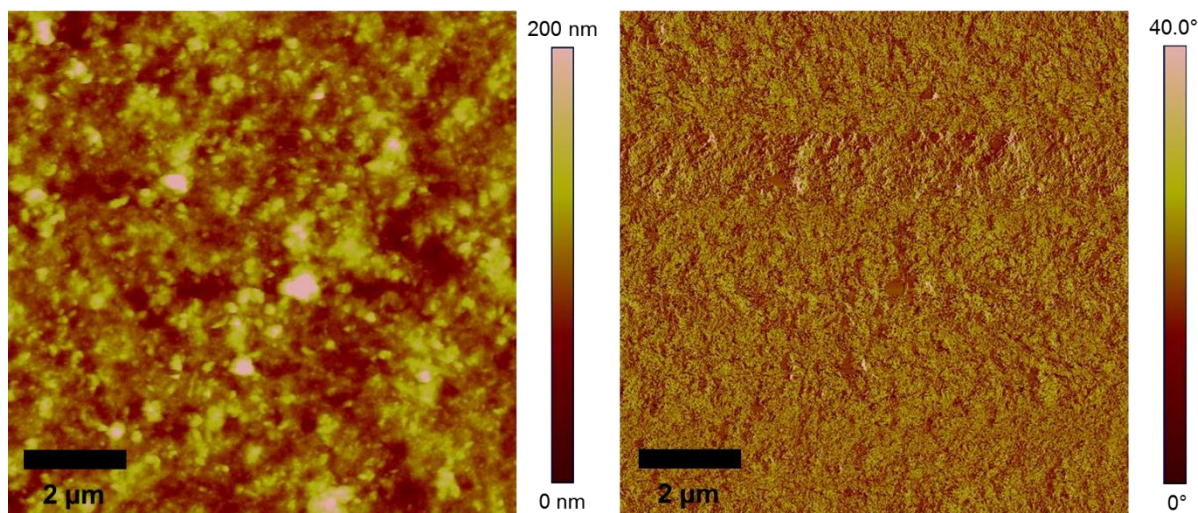

Figure 23: Topography image (left) and phase image (right) of the solar cell displayed with AFM

In the topography image it can be detected that the surface is rather rough due to the agglomeration of the CIS nanocrystals in the polymer. In the phase image a rather irregular distribution of the nanocrystals can be detected which underlines the observation in the topography image.

3.2.1.4.4 I/V measurements

The bulk heterojunction solar cells were built as described in 4.3.2 and the active layer was prepared as described in 4.3.4.1.

The solar cells were prepared with an active layer containing a polymer to CIS ratio of 1:9 and a polymer concentration of 5 mg/ml. In pre-experiments various rotation speeds of spin coating were tested where 1500 rpm proved to be the option for an optimal thickness for a good performance of the solar cell and therefore high efficiency. The resulting devices had an average PCE of 0.21 ± 0.01 %. Both, the V_{OC} (0.716 ± 0.035 V) as well as the I_{SC} (1.093 ± 0.069 mA/cm²) were rather high for this setup. The measured thickness of the active layer was around 92 nm. A representative I/V diagram of the solar cell of this preparation with the best performance is shown in Figure 24.
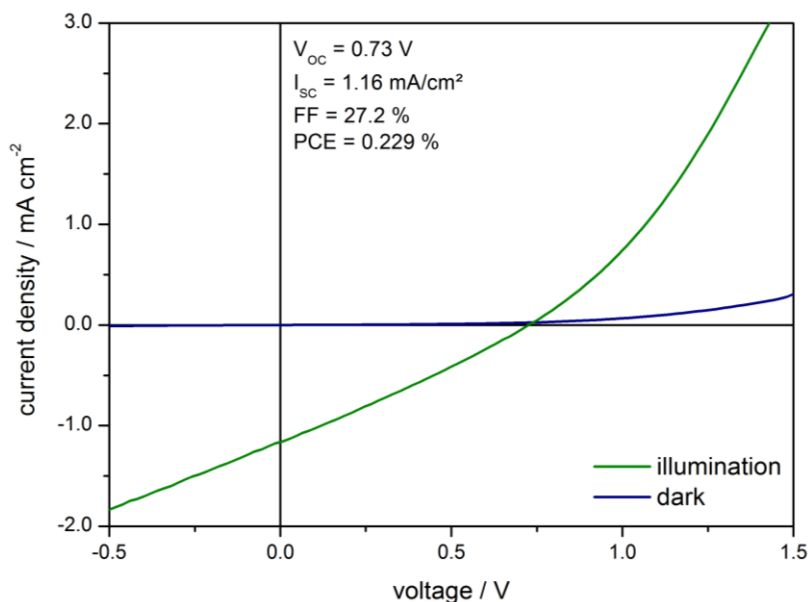
Figure 24: I/V diagram of the solar cell with best performance with polymer to CIS ratio of 1:9, not tempered

To find out if the performance and therefore the efficiency of the solar cells with this setup can be influenced in a positive fashion via annealing, devices with the same setup were prepared and tempered at 140 °C for 10 min after the deposition of the active layer. This step led to a slight decrease of all parameters instead of a desired increase. These devices had a V_{OC} of 0.510 ± 0.072 V, a I_{SC} of 1.009 ± 0.032 mA/cm² and a PCE of 0.13 ± 0.02 %. In Figure 25 the I/V curve of the solar cell of this preparation with the best performance is shown.

Figure 25: I/V diagram of the solar cell with best performance with polymer to CIS ratio of 1:9, tempered

For comparison active layers with a polymer to CIS ratio of 1:5 were prepared in the same fashion as the first solar cells with a ratio of 1:9. The thickness of the active layer was reduced to about 40 nm. The devices had a V_{OC} of 0.327 ± 0.182 V, a I_{SC} of 1.684 ± 0.306 mA/cm² and a PCE of $1.3*10^{-2} \pm 7*10^{-3}$ %. The average poor performance of the solar cells can be explained

by the rather thin thickness of the active layer and the lack of CIS nanocrystals for the generation of enough excitons. The I/V curves of the solar cell of this preparation with the best performance is shown in Figure 26.

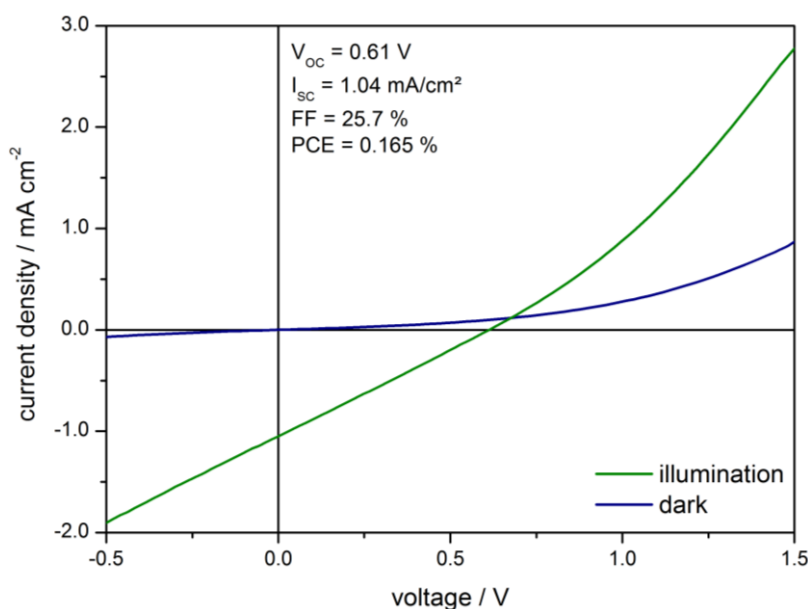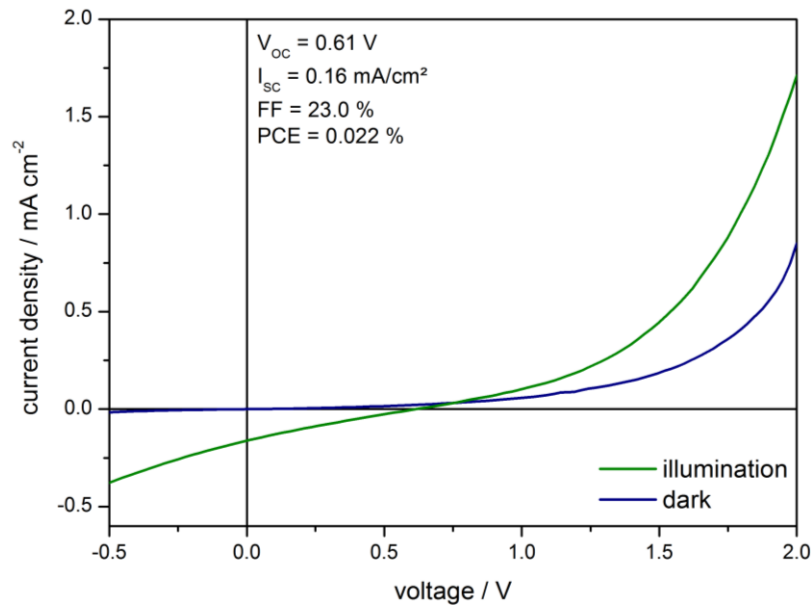**Figure 26: I/V diagram of the solar cell with best performance with polymer to CIS ratio of 1:5, not tempered**

Further solar cells with an active layer of an increased polymer to CIS ratio of 1:15 were prepared to find out if the performance can be improved. The active layers had a thickness of about 142 nm which is a slight increase compared to those with a ratio of 1:9. The devices had a V_{OC} of 0.224 ± 0.083 V, a I_{SC} of 0.888 ± 0.014 mA/cm² and a PCE of $5*10^{-3} ± 2*10^{-3}$ %. The resulting average unexpected very poor performance might be due to the reduction of polymer in the active layer to about 20% due to the increase of CIS nanocrystals. The nanocrystals did also not dissolve properly in the polymer solution and this led to a much rougher surface of the film. The charge transfer may also be influenced negatively. In Figure 27 the I/V diagram of the solar cell of this preparation with the best performance is shown.
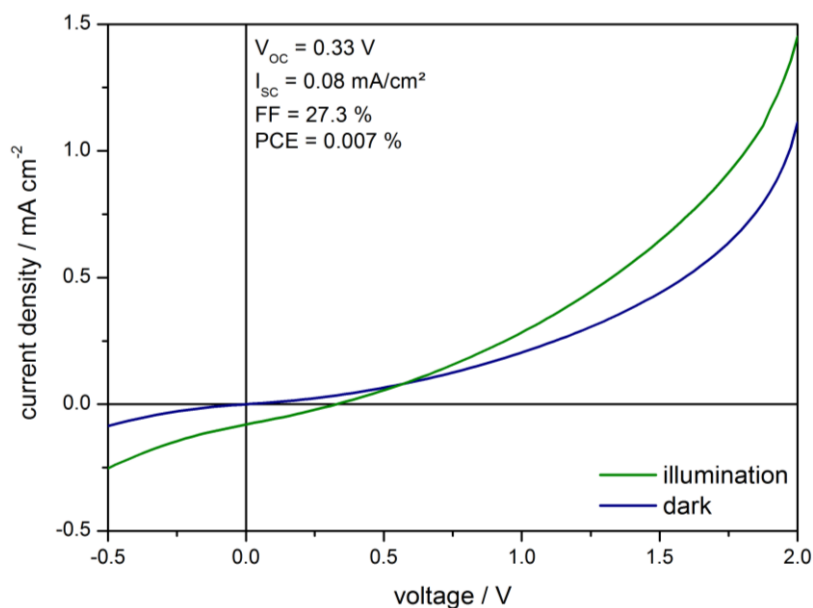
Figure 27: I/V diagram of the solar cell with best performance with polymer to CIS ratio of 1:15, not tempered

3.2.2 Ligand exchange with ammonium thiocyanate

Many ligands used for ligand exchange cause problems such as for example toxicity. Ammonium thiocyanate is environmentally harmless, air-stable and worldwide produced in kiloton scale. A negative aspect is that it is hazardous for the human health. The ligand SCN is very short and can be used in solution as well as solid-state ligand exchange. Additionally, it is suitable for a wide range of semiconductor and metal nanocrystals.[32]

3.2.2.1 Syntheses methods

Due to the small diameter of the CIS nanocrystals gained with the method described in chapter 4.1.4 various other syntheses methods were tested before a ligand exchange with ammonium thiocyanate. Here it was intended to get CIS nanocrystals with a higher diameter by changing the capping agents or the reaction conditions. The capping agent was changed from a 1:1 mixture of oleyl amine and oleic acid (dioleamide; chapter 4.1.4)[38], to only oleic acid (chapter 4.1.3), to a 2:8 mixture of oleyl amine and octadecene (chapter 4.1.7)[30] and to a 1:9 mixture of oleyl amine and oleic acid (chapter 4.1.6)[38], respectively. Additionally, the influence of heating the reaction mixture under controlled conditions (time and temperature) in a synthesis reactor (see chapter 4.4.10) on the particle size was investigated. This approach was performed using the capping agents dioleamide (chapter 4.1.9)[38] and oleylamine (chapter 4.1.8), respectively. Lastly, it was examined how further addition of precursors (doubled precursor) will have an impact on the particle size (chapter 4.1.5).

All the syntheses yielded $CuInS_2$ nanocrystals which can be seen in the XRD patterns (Figure 28).
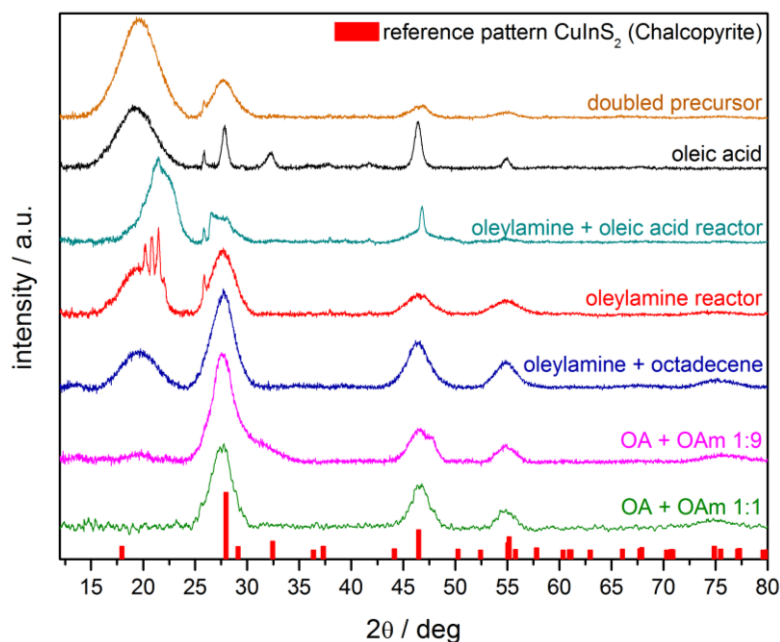
Figure 28: XRD patterns of CIS nanocrystals synthesized by various methods

From the XRD patterns shown it can be concluded that the synthesized CIS nanocrystals have a chalcopyrite structure. The three main peaks are at 28° (112), 46° (220) and 55° ((116) and (312)). The diameters of the nanocrystals were estimated by the Scherrer equation (Equation 1, chapter 3.1.). Against expectations the diameter of the particles did not change much and were in the range of the synthesis using dioleamide as capping agent (3.4-4.1 nm; see chapter 3.1.). The estimated diameters for each synthesis are summarized in Table 2. Only the synthesis where only oleic acid was used as capping agent (chapter 4.1.3) nanocrystals with diameters between 13 and 20.6 nm were yielded.

Table 2: estimated diameters of CIS nanocrystals synthesized by different methods

Synthesis method	Diameter of nanocrystals
doubled precursor	2.9 - 3.9 nm
oleic acid	13.0 - 20.6 nm
oleylamine + oleic acid (1:1) reactor	3.0 - 4.1 nm
oleylamine reactor	2.3 - 3.3 nm
oleylamine + octadecene (2:8)	3.3 - 3.8 nm
oleylamine + oleic acid (1:9)	3.3 - 4.5 nm
oleylamine + oleic acid (1:1)	3.4 - 4.0 nm

3.2.2.2 Analysis of ligand exchange

The ligand exchange with ammonium thiocyanate as described in chapter 4.2.5 was conducted with the CIS nanocrystals gained by the methods using dioleamide and oleic acid as capping agent, respectively. Due to the insolubility of the ligand exchanged (former oleic acid capped)

nanocrystals in chloroform and chlorobenzene (desired for the incorporation in solar cells) only the ligand exchange of the former dioleamide capped nanocrystals was further analyzed.

3.2.2.2.1 *FTIR spectroscopy*

To confirm if the ligand exchange has worked properly, FTIR spectroscopy was performed. The results of the analysis are shown in Figure 29.
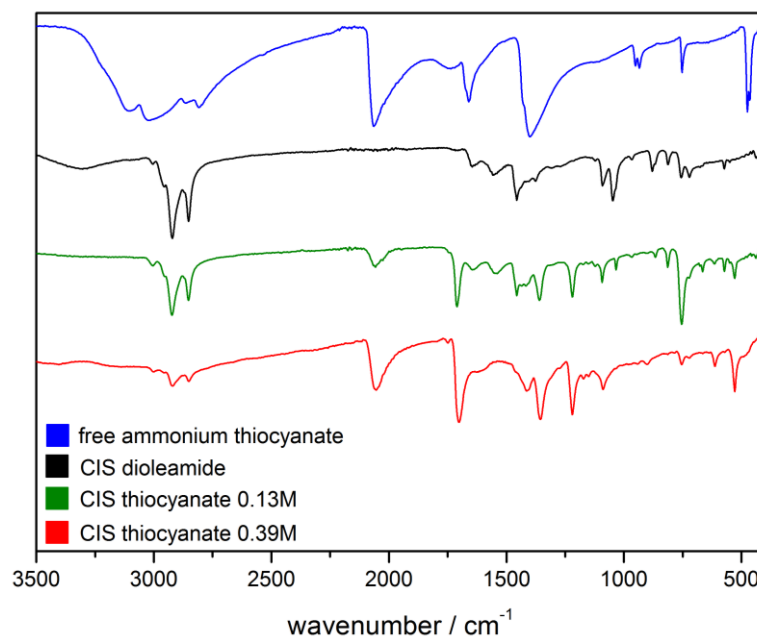

Figure 29: IR spectra of dioleamide and thiocyanate capped CIS ligand exchanged with different concentrations of NH₄SCN

As already explained in chapter 3.2.1.1. the wavenumbers at 1558, 1644, 3005 and 3260 cm^{-1} in the spectra of the non-ligand exchanged CIS nanocrystals can be attributed to dioleamide and are hardly present in the spectra of the thiocyanate capped CIS nanocrystal samples. The bands at 1458, 2852, 2921 and 2954 cm^{-1} which correspond to the scissor vibration of the C-H-bond, the asymmetric and symmetric stretching vibration of the C-H bond are present in the sample of dioleamide capped CIS and get weaker in the samples of ligand exchanged CIS. In the sample of CIS exchanged with higher concentration of NH₄SCN these bands are very weak. The unique band for NH₄SCN at 2064 cm^{-1} corresponds to the asymmetric stretching vibration of the N≡C-S^{-} ion. This is one of two bands present in the sample of free ammonium thiocyanate and the samples of ligand-exchanged CIS. Due to the adsorption on the nanocrystals it is shifted to 2054 cm^{-1}. The strong band at 1660cm^{-1} can be attributed to the symmetric stretching vibration of C=N, in the samples of ligand-exchanged CIS it is shifted to 1700cm^{-1}. The mentioned bands of the four samples are summarized in Table 3.

Table 3: assignment of IR bands of thiocyanate and dioleamide adsorbed on CIS[45]

free ammonium thiocyanate	
wave number [cm^{-1}]	**vibrations**
1399	δ(N-H)
1660	v_s(C=N)
2064	v_{as}(N≡C-S$^-$)
2807-3107	v_{as}(N-H) & v_s(N-H)
dioleamide adsorbed on CIS	
1458	scissor vib. (C-H) in R_2-CH$_2$
1558	δ(N-H)
1644	δ(-C=C) + v(C=O)
2852	v_{as}(C-H)
2921	v_s(C-H)
2954	v_s(C-H)
3005	δ(=C-H)
3260	v(N-H)
thiocyanate adsorbed on CIS	
1700	v_s(C=N)
2054	v_{as}(N≡C-S$^-$)
2852	v_{as}(C-H)
2921	v_s(C-H)

3.2.2.2.2 Thermogravimetric analysis

For determination of the amount of capping agent adsorbed onto the CIS nanocrystals a thermogravimetric analysis was conducted. Two measurements of the nanocrystals were done, before and after the ligand exchange (Figure 30). Here only the result of the ligand exchange with a higher concentration of NH_4SCN (0.39 M) is displayed due to the positive result in the IR measurement and in the therefore motivated further work with these particles.
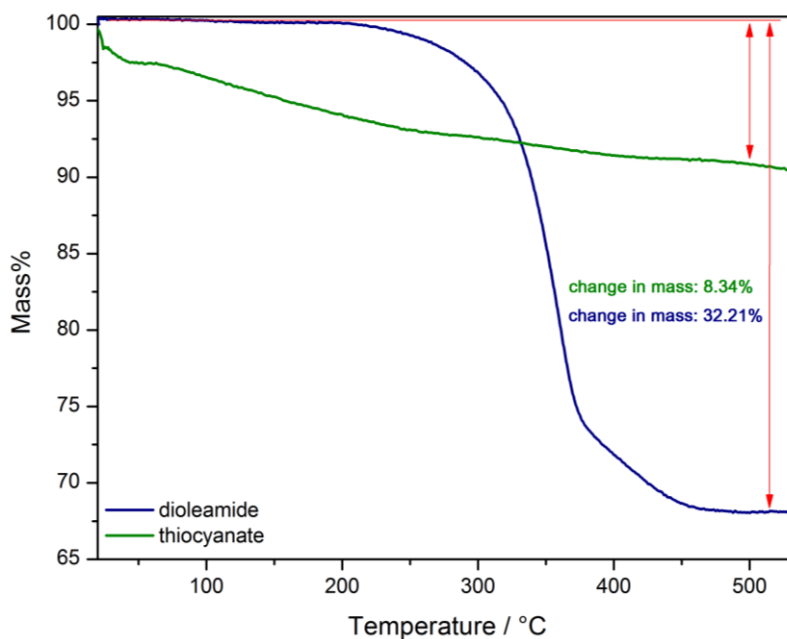
Figure 30: TGA curve of CIS nanocrystals before and after ligand exchange with ammonium thiocyanate

The measured mass loss refers to the amount of the capping agents of the nanocrystals.

In the sample of thiocyanate capped CIS nanocrystals, the mass loss between 50 and 250°C can be ascribed to free ammonium thiocyanate still present in the sample after the precipitation step. The mass loss above 300°C in both samples can be explained by the decomposition of dioleamide and thiocyanate which are coordinated on the CIS nanocrystals, respectively. The huge difference in mass loss is due to the much lower mass of thiocyanate compared to dioleamide. Due to the smaller head group of thiocyanate compared to dioleamide, more molecules can coordinate on the nanocrystal surface.

3.2.2.3 Incorporation of nanocrystals in hybrid solar cell

The aim of the incorporation of the CIS nanocrystals in quantum-dot sensitized solar cells was to test their applicability in this type of solar cell. Various polymers were investigated and the influence of the amount of CIS nanocrystals was tested. The overall results of the optimization of the devices are shown below. The presented results of open circuit voltage (V_{OC}), short circuit current (I_{SC}), fill factor (FF) and power conversion efficiency (PCE) are the average of the five best cells if not stated differently.

Solar cells with the assembly of a semiconductor sensitized solar cell were built. The CIS nanocrystals acted as donor material and the conjugated polymer poly(3-hexylthiophene-2,5-diyl) (P3HT) was used as hole transport layer. PCDTBT and Spiro-OMeTAD were also tested as hole transport layer, but they worked much worse than the solar cells with P3HT.

3.2.2.3.1 Absorption measurement of active layer

For the determination of the absorption properties of the active layer they were investigated by UV/Vis spectroscopy as described in chapter 4.4.2. In Figure 31 the absorption spectra of one

to eleven layers of CIS nanocrystals on mesoporous TiO_x are shown. In addition, a picture of the substrates with increasing CIS layers mentioned before is shown in Figure 32.
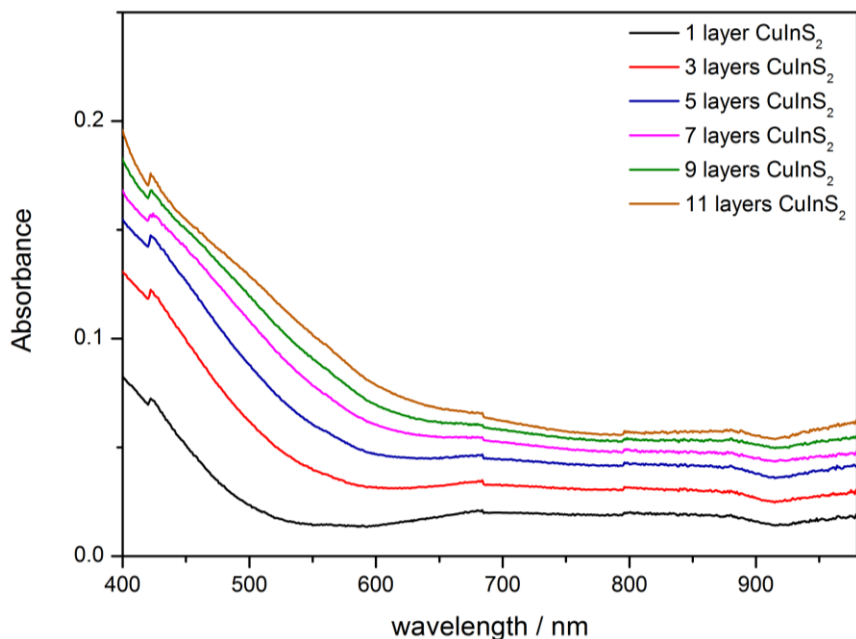

Figure 31: UV/Vis spectra of various numbers of layers of CIS nanocrystals on mesoporous TiO_x

By comparing the samples with increasing number of CIS layers an increase in absorption can be detected, due to the increase in CIS content and therefore in layer thickness. At lower wavelength the differences in absorption of the samples are higher and the absorbance increases up to 0.2. With increasing number of CIS layers the onset of the absorption is shifted to higher wavelengths.

Figure 32: Substrates with increasing number of layers of CIS nanocrystals on TiO_x (left to right: 1,3, 5, 7, 9, 11)

Figure 32 shows clearly why the absorbance of the layers of CIS nanocrystals is that weak. With only one layer hardly any brown coloration can be detected whereas with eleven layers a slight change in color can be seen.

Absorption spectra of the active layer with one and eleven layers of CIS nanocrystals and P3HT, respectively, are shown in Figure 33. After spin coating a layer of P3HT on the substrates with one and eleven layers of CIS nanocrystals as described in chapter 4.4.2 only a slight difference in absorbance could be detected (Figure 33). The sample with only one layer of CIS nanocrystals can here be seen like a pure P3HT sample. With eleven layers of CIS a slight increase in absorbance can be detected at wavelengths below 500 nm and above

650 nm. P3HT has its absorption maximum at 515 nm and hardly absorbs after 700 nm. The samples had a difference in thickness of around 100 nm.
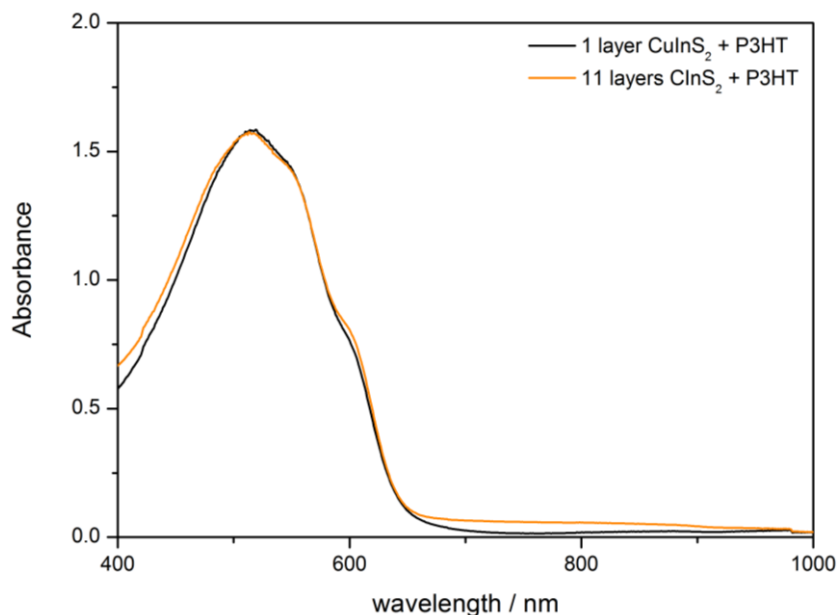

Figure 33: UV/Vis spectra of one and 11 layers of CIS nanocrystals with additional P3HT layer

3.2.2.3.2 I/V measurements

The quantum-dot sensitized solar cells were built as described in 4.3.3 and the hole transport layer was prepared as described in 4.3.4.2.

In pre-experiments various rotation speeds of spin coating of mesoporous TiO_x were tested to gain a variety of layer thickness. The combination of a rotation speed of 6000 rpm and a velocity of 3000 rpm/s delivered a thickness of about 160 nm and proved to be the options for an optimal thickness for a good performance of the solar cell and therefore high efficiency. As already mentioned in chapter 3.2.2 beside P3HT, PCDTBT and Spiro-OMeTAD were tested as hole transport layer but worked worse with CIS nanocrystals in this setup. Therefore, P3HT was used for further experiments.

Substrates with different concentrations of P3HT were examined. As it can be seen in Table 4 the performance of the solar cells increased with increasing concentration.

Table 4: average characteristic parameters of solar cells with only P3HT in different concentrations

	15 mg/ml	**25 mg/ml**	**30 mg/ml**
V_{OC} [V]	0.075 ± 0.021	0.592 ± 0.310	0.813 ± 0.104
I_{SC} [mA/cm^2]	0.316 ± 0.039	0.504 ± 0.032	0.601 ± 0.022
PCE [%]	$7*10^{-3} \pm 4*10^{-3}$	0.197 ± 0.111	0.279 ± 0.060

It was decided to use a polymer concentration of 30 mg/ml for further the solar cells.

To find out if different amounts of CIS nanocrystals influence the performance of the solar cells substrates with one, three and five layers of CIS nanocrystals were prepared before applying

the P3HT layer. In Table 5 the characteristic parameters of the different layers are listed. With increasing CIS amount no improvement in performance can be detected. The cells were measured again after 24 hours and a slight increase in performance was noticed. Mostly the parameters of the solar cells with one layer of CIS nanocrystals increased.

Table 5: average characteristic parameters of solar cells with different number CIS NP layers and P3HT layer

	1 CIS NP layer	3 CIS NP layers	5 CIS NP layers
V_{OC} [V]	0.498 ± 0,226	0.556 ± 0.010	0.576 ± 0.012
I_{SC} [mA/cm^2]	1.699 ± 0.048	1.433 ± 0.305	1.438 ± 0.028
FF [%]	38.82 ± 8.42	39.27 ± 2.13	44.56 ± 1.15
PCE [%]	0.361 ± 0.186	0.317 ± 0.035	0.358 ± 0.013
after 24 hours			
V_{OC} [V]	0.630 ± 0.011	0.551 ± 0.012	0.561 ± 0
I_{SC} [mA/cm^2]	2.223 ± 0.058	1.866 ± 0.091	1.520 ± 0.066
FF [%]	51.43 ± 1.40	41.77 ± 0.021	45.17 ± 1.29
PCE [%]	0.710 ± 0.037	0.446 ± 0.050	0.376 ± 0.024

Due to the rather low characteristic parameters and minor improvement in contrast to the pure polymer it was expected that the performance and therefore the efficiency of the solar cells could be improved via annealing. Devices with the same setup and with one and three layers of CIS nanocrystals were prepared, respectively, and tempered at 200 °C for 5 min before the deposition of the polymer. Herewith the residual solvent dimethyl formamide should be evaporated due to a boiling point at 153 °C. Surprisingly, all characteristic parameters of the solar cells using one and three layers of CIS nanocrystals, respectively decreased after the annealing. After 24 hours the cells were measured again and the performance increased slightly.

Table 6: average characteristic parameters of solar cells with one & three CIS NP layers and P3HT layer after annealing

	1 CIS NP layer	3 CIS NP layers
V_{OC} [V]	0.490 ± 0.010	0.379 ± 0.010
I_{SC} [mA/cm^2]	1.446 ± 0.050	1.147 ± 0.046
FF [%]	44.89 ± 0.79	33.41 ± 0.72
PCE [%]	0.308 ± 0.012	0.143 ± 0.007
after 24 hours		
V_{OC} [V]	0.490 ± 0.010	0.379 ± 0.010
I_{SC} [mA/cm^2]	1.434 ± 0.064	1.282 ± 0.042
FF [%]	0.461 ± 0.008	33.93 ± 0.74
PCE [%]	0.313 ± 0.010	0.158 ± 0.007

As a second step an additional treatment of the layers of CIS nanocrystals with $InCl_3$ (0.5 mg/ml in THF) was tested. Here devices with the same setup and one and three layers of CIS nanocrystals, respectively, were prepared. After coating and annealing each layer of CIS at 200 °C for 5 min 20μl of the $InCl_3$ solution were distributed on the substrates and spun off. Afterwards the layer of P3HT was applied onto the substrates. The cells were also measured after 24 hours. All characteristic parameters of the solar cells using one and three layers of CIS nanocrystals, respectively, decreased further compared to those of the untreated and the annealed solar cells. After 24 hours no improvement could be detected.

Table 7: average characteristic parameters of solar cells with one & three CIS NP layers and P3HT layer after annealing and InCl₃ treatment

	1 CIS NP layer	3 CIS NP layers
V_{OC} [V]	0.222 ± 0.047	0.163 ± 0.011
I_{SC} [mA/cm²]	0.633 ± 0.117	1.495 ± 0.186
FF [%]	36.41 ±1.93	30.36 ± 2.09
PCE [%]	0.051 ± 0.021	0.071 ± 0.011
after 24 hours		
V_{OC} [V]	0.177 ± 0.061	0.125 ± 0.011
I_{SC} [mA/cm²]	0.953 ± 0.136	1.053 ± 0.104
FF [%]	28.12 ± 1.46	26.70 ± 1.66
PCE [%]	0.041 ± 0.026	0.034 ± 0.005

The annealing step and the $InCl_3$ treatment, both did not deliver the desired improvement on the performance of the solar cells. In Figures 34 and 35 a comparison of all I/V curves of the best cells of the substrates using one and three layers of CIS nanocrystals, respectively, and their treatments are shown.
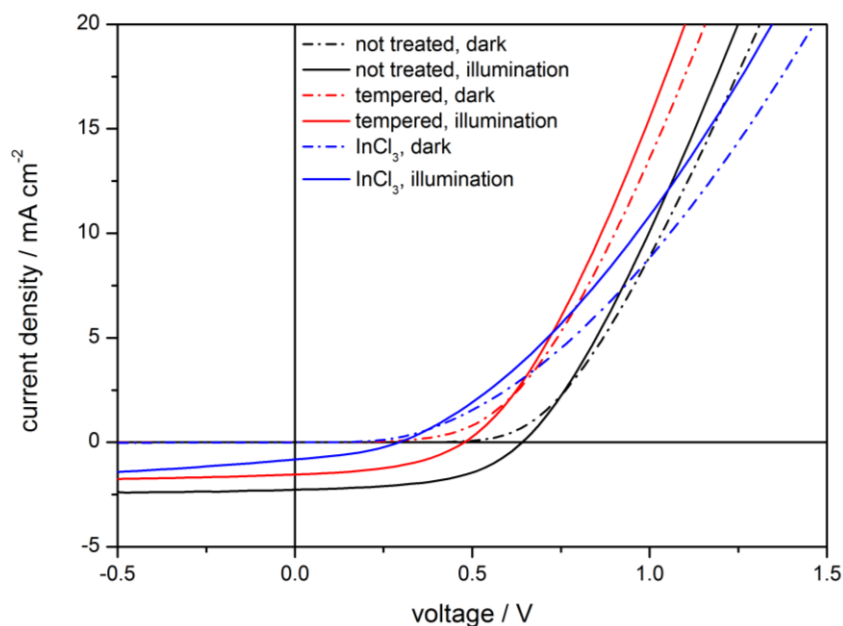

Figure 34: I/V curves of the best cells using one layer of CIS nanocrystals and different treatments
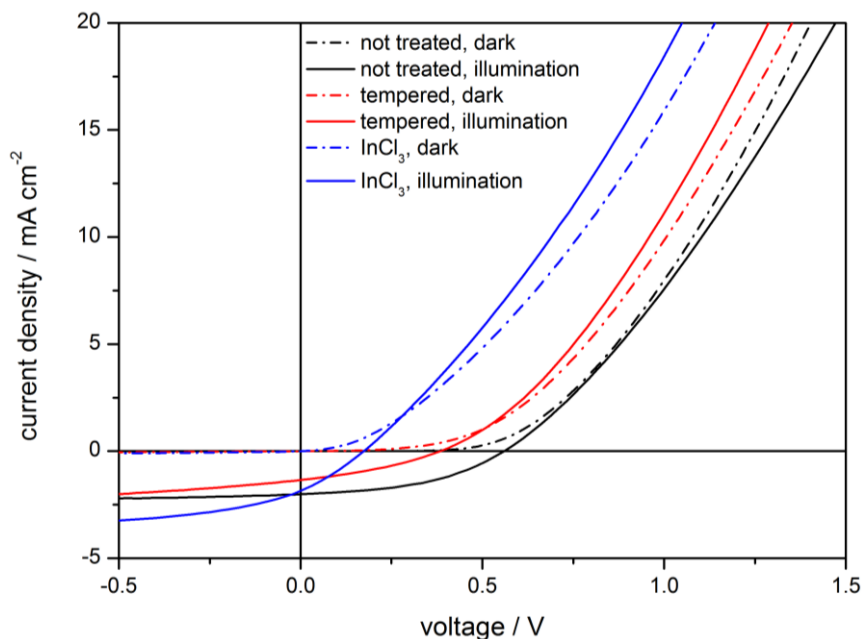
Figure 35: I/V curves of the best cells using three layers of CIS nanocrystals and different treatments

A comparison of the best cells with one and three CIS layers and pure P3HT can be seen in Figure 36.
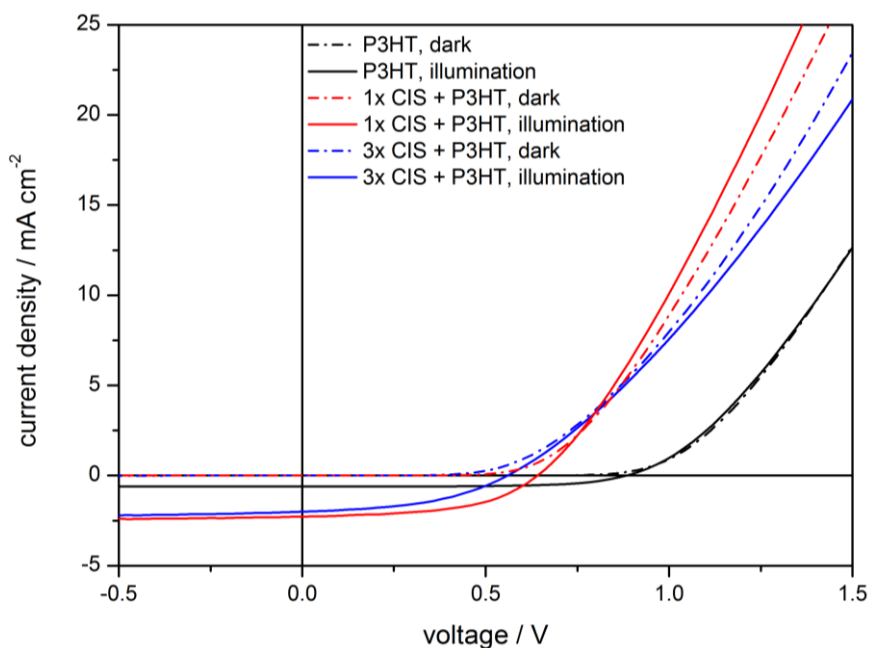

Figure 36: I/V curves of the best cells using one and three layers of CIS nanocrystals, respectively compared to pure P3HT

By comparing the values for the characteristic parameters for pure P3HT, one layer and three layers of CIS nanocrystals (Table 4 and 5) no clear improvement could be made by increasing the number of CIS layers. With pure P3HT the highest values for V_{OC} could be reached, whereas by adding only one layer of CIS the highest values for I_{SC} could be obtained. The highest PCE of the solar cells was gained by using one CIS layer.

3.2.2.3.3 External quantum efficiency (EQE)

The external quantum efficiency is the ratio of the number of electrons collected by the solar cell to the number of incident photons.

The EQE spectra for the best cells using one and three layers of CIS nanocrystals are shown in Figure 37. The measured absorption of the CIS nanocrystals was very low, so the efficiency in the wavelength region between 400 and 650 nm can be only contributed to the polymer P3HT. Charge carriers generated in the polymer, due to light absorption, contribute to the photocurrent. Comparing the cells with one and three layers of nanocrystals a decrease in charge carriers can be detected with more nanocrystals. This was also seen during I/V measurements and might be due to a decrease of the interface between nanocrystals and P3HT. Out of these results it can be concluded that no quantum-dot sensitized solar cell could be built. If this would be the case the EQE would also be higher at the wavelengths until 850 nm where the nanocrystals have their onset in absorbance.
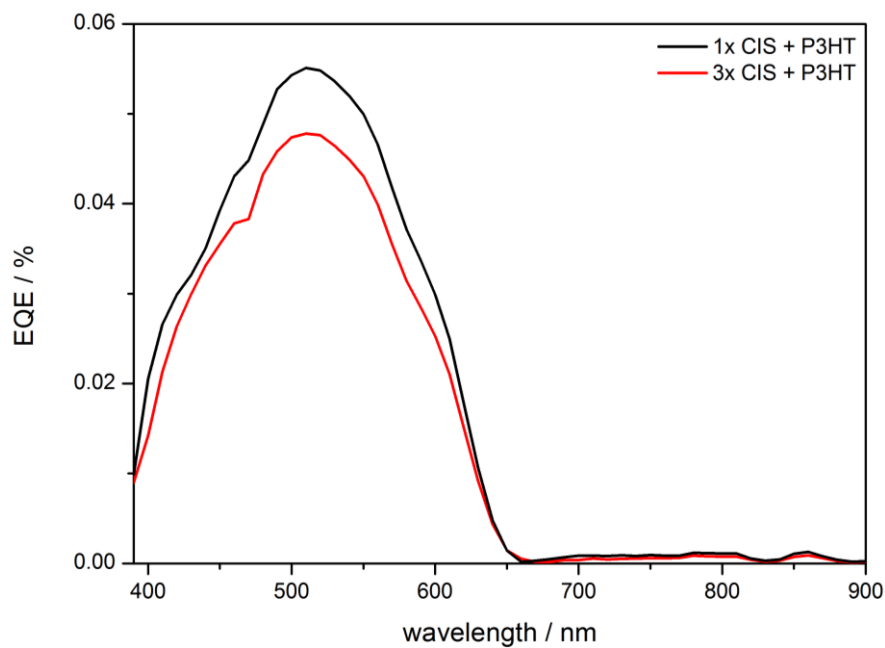

Figure 37: EQE spectra of solar cells using one and three layers of CIS nanocrystals

4   Experimental

4.1   Synthesis of copper indium disulfide nanocrystals

4.1.1   Heat-up method – octadecene/oleylamine (70:30) and dodecanethiol

In a three-necked flask 181.6 mg (1 mmol) Cu(OAc), 496.3 mg (1.7 mmol) In(OAc)$_3$ and 1.356 g (3.5 mmol) trioctylphosphine oxide (TOPO) were dissolved in a mixture of 7 ml octadecene (ODE) and 3 ml oleylamine (OAm) under N$_2$ atmosphere which resulted in a green solution. For 30 minutes N$_2$ is bubbled through the solution which turns to blue-green. The reaction mixture is heated to 200 °C (100 °C: royal blue; ca. 160 °C: dark cyan; 200 °C: yellow-green, opaque). A mixture of 0.25 ml 1-dodecanethiol and 1.75 ml *tert*-dodecanethiol is rapidly injected into the reaction mixture whose color changes to light brown-orange. The mixture was heated to 240 °C. After one hour, the reaction product was left to cool down to room temperature. Ethanol (volume ratio of 2:1 to reaction product) was poured into a centrifuge tube and the reaction product was added. The nanocrystals were separated by centrifugation at 3600 rpm for 5 minutes. The clear, yellowish supernatant was decanted and 20 ml ethanol was added to the black precipitate. The nanocrystals were separated by centrifugation at 3600 rpm for 5 minutes. The clear supernatant was decanted and the remaining nanocrystals were dissolved in 5 ml chloroform resulting in a black-brown solution.

4.1.2   Hot injection method – oleylamine

In a three-necked flask 30 ml OAm was heated to 200 °C under N$_2$ atmosphere. 191.3 mg (0.75 mmol, 1 eq.) copper O-2,2-dimethylpentan-3-yl dithiocarbonate (CuHep) and 1.172 g (1.7 mmol, 2.26 eq.) indium O-2,2-dimethylpentan-3-yl dithiocarbonate (InHep) were dissolved in 6.5 ml 1,2,4-trichlorobenzene. Subsequently, the prepared precursor solution was injected via a syringe into the hot oleylamine. The reaction mixture gets black-brownish immediately. After one hour, the black reaction product was left to cool down to room temperature. Methanol (volume ratio of 2:1 to reaction product) was poured into two centrifuge tubes and the reaction product was added. The nanocrystals were separated by centrifugation at 3600 rpm for 5 minutes. The clear supernatant was decanted and the remaining nanocrystals were dissolved in 6 ml chloroform resulting in a black-brown solution. The precipitation step was repeated a second time.

4.1.3   Hot injection method – oleic acid

In a three-necked flask 30 ml oleic acid (OA) was heated to 185 °C under N$_2$ atmosphere. 191.5 mg (0.75 mmol, 1 eq.) CuHep and 1.171 g (1.7 mmol, 2.26 eq.) InHep were dissolved in 6.5 ml 1,2,4-trichlorobenzene. Subsequently, the prepared precursor solution was injected via a syringe into the hot oleic acid. The reaction mixture gets black immediately. After 30 minutes, the black reaction product was left to cool down to room temperature.

For precipitation, the following precipitation agents were tested:

- ethanol
- ethanol/n-hexane (1:1)
- ethanol/isopropanol (1:1)

The precipitation was accomplished using a mixture of ethanol and isopropanol with a volume ratio of 1:1. The solvent mixture (volume ratio of 2:1 to reaction product) was poured into two centrifuge tubes and the reaction product was added. The nanocrystals were separated by centrifugation at 3600 rpm for 5 minutes. The clear supernatant was decanted and the remaining nanocrystals were dissolved in chloroform resulting in a black-grey solution.

4.1.4 Hot injection method – oleylamine/oleic acid (50:50)

In a three-necked flask 15 ml OAm and 15 ml OA were heated to 200 °C under N_2 atmosphere. 191.2 mg (0.75 mmol, 1 eq.) CuHep and 1.171 g (1.7 mmol, 2.26 eq.) InHep were dissolved in 6.5 ml 1,2,4-trichlorobenzene. Subsequently, the prepared precursor solution was injected via a syringe into the hot reaction mixture which gets black-brownish immediately. After 30 minutes, the black reaction product was left to cool down to room temperature. Methanol (volume ratio of 2:1 to reaction product) was poured into two centrifuge tubes and the reaction product was added. The nanocrystals were separated by centrifugation at 3600 rpm for 5 minutes. After centrifugation, a 3-phase mixture was received: black precipitant – black, opaque solution – clear, solution with white streaks. A mixture of 20 ml n-hexane and 20 ml ethanol was poured into a centrifuge tube and the black solution of the 3-phase mixture was added. The nanocrystals were separated by centrifugation at 3600 rpm for 5 minutes. The clear supernatant was decanted and the remaining nanocrystals together with the black precipitant were dissolved in 8 ml chloroform. The nanocrystals were precipitated again with 16 ml methanol, centrifuged as described above and dissolved in chloroform resulting in a black-brown solution.

4.1.5 Hot injection method – oleylamine/oleic acid (50:50) doubled precursor

In a three-necked flask 15 ml OAm and 15 ml OA were heated to 185 °C under N_2 atmosphere. 191 mg (0.75 mmol, 1 eq.) CuHep and 1.172 g (1.7 mmol, 2.26 eq) InHep were dissolved in 6.5 ml 1,2,4-trichlorobenzene. Subsequently, the prepared precursor solution was injected via a syringe into the hot reaction mixture which gets black-brownish immediately. After 10 minutes, a solution of 190.8 mg (0.75 mmol, 1 eq.) CuHep and 1.168 g (1.7 mmol, 2.26 eq.) InHep dissolved in 6.5 ml 1,2,4-trichlorobenzene is dropped into the reaction mixture over 5 minutes. The black reaction product was left to cool down to room temperature. A mixture of ethanol and n-hexane with a volume ratio of 1:1 (volume ratio of 2:1 to reaction product) was poured into two centrifuge tubes and the reaction product was added. The nanocrystals were separated by centrifugation at 3600 rpm for 5 minutes. The clear supernatant was decanted

and the remaining nanocrystals were dissolved in chloroform resulting in a black-brown solution.

4.1.6 Hot injection method – oleylamine/oleic acid (10:90)

In a three-necked flask 27 ml OA and 3 ml OAm were heated to 185 °C under N_2 atmosphere. 191.2 mg (0.75 mmol, 1 eq.) CuHep and 1.171 g (1.7 mmol, 2.26 eq.) InHep were dissolved in 6.5 ml 1,2,4-trichlorobenzene. Subsequently, the prepared precursor solution was injected via a syringe into the hot reaction mixture which gets black-brownish immediately. After 30 minutes, the black reaction product was left to cool down to room temperature. A mixture of ethanol and isopropanol with a volume ratio of 1:1 (volume ratio of 2:1 to reaction product) was poured into two centrifuge tubes and the reaction product was added. The nanocrystals were separated by centrifugation at 3600 rpm for 5 minutes. The clear supernatant was decanted and the remaining nanocrystals were dissolved in chloroform resulting in a black-brown solution.

4.1.7 Hot injection method – octadecene/oleylamine (80:20)

In a three-necked flask 24 ml ODE and 6 ml OAm were heated to 185 °C under N_2 atmosphere. 191.1 mg (0.75 mmol, 1 eq.) CuHep and 1.170 g (1.7 mmol, 2.26 eq.) InHep were dissolved in 6.5 ml 1,2,4-trichlorobenzene. Subsequently, the prepared precursor solution was injected via a syringe into the hot reaction mixture which gets black immediately. After 30 minutes, the black reaction product was left to cool down to room temperature. Ethanol (volume ratio of 2:1 to reaction product) was poured into two centrifuge tubes and the reaction product was added. The nanocrystals were separated by centrifugation at 3600 rpm for 5 minutes. After centrifugation, a 2-phase mixture was received: black, opaque solution – clear solution.

For precipitation, the following precipitation agents were tested:

- ethanol/n-hexane (1:1)
- ethanol/isopropanol (1:1)

The precipitation was accomplished using a mixture of ethanol and isopropanol with a volume ratio of 1:1. The solvent mixture (volume ratio of 2:1 to reaction product) was poured into two centrifuge tubes and the black solution of the 2-phase mixture was added. The nanocrystals were separated by centrifugation at 3600 rpm for 5 minutes. The clear supernatant was decanted. The remaining nanocrystals did not dissolve in chloroform.

4.1.8 Heat-up method in synthesis reactor – oleylamine

19.2 mg (0.75 mmol, 1 eq.) CuHep and 117 mg (1.7 mmol, 2.26 eq.) InHep were dissolved in 0.65 ml 1,2,4-trichlorobenzene. 3 ml OAm is filled into a small reactor vessel and the dissolved precursors were added. This resulted in an orange solution which turned red after 5 minutes

at room temperature. The reaction mixture was introduced in a reactor (see chapter 4.4.10) and was subjected to the following heat program:

- 25 °C to 100 °C in 10 min
- 100 °C to 200 °C in 99 min
- hold 200 °C for 60 min

Methanol (volume ratio of 2:1 to reaction product) was poured into a centrifuge tube and the black-brown reaction product was added. The nanocrystals were separated by centrifugation at 3000 rpm for 5 minutes. The clear supernatant was decanted and the remaining nanocrystals were dissolved in chloroform resulting in a black-brown solution.

4.1.9 Heat-up method in synthesis reactor – oleylamine/oleic acid (50:50)

19.2 mg (0.75 mmol, 1 eq.) CuHep and 117 mg (1.7 mmol, 2.26 eq.) InHep were dissolved in 0.65 ml 1,2,4-trichlorobenzene. 1,5 ml OAm and 1,5 ml OA were filled into a small reactor vessel and the dissolved precursors were added. This resulted in an orange-brownish solution at RT. The reaction mixture was introduced in a reactor (see chapter 4.4.10) and was subjected to the following heat program:

- 25 °C to 100 °C in 10 min
- 100 °C to 200 °C in 99 min
- hold 200 °C for 60 min

A mixture of ethanol and n-hexane with a volume ratio of 1:1 (volume ratio of 2:1 to reaction product) was poured into a centrifuge tube and the viscous, black-brown reaction product was added. The nanocrystals were separated by centrifugation at 3000 rpm for 5 minutes. The clear supernatant was decanted and the remaining nanocrystals were dissolved in chloroform resulting in a black-brown solution.

4.2 Ligand exchange

4.2.1 Ligand exchange with pyridine

A specific amount of CIS nanocrystals, which were prepared as depicted in chapters 4.1.1, 4.1.2 and 4.1.4 was dissolved in pyridine. The exact values of CIS particles and pyridine used are listed in Table 8. All reactions were performed at 80 °C. After 24 hours, the solutions were left to cool down to room temperature. A mixture of ethanol and acetone with a volume ratio of 1:1 (volume ratio of 2:1 to reaction product) was poured into two centrifuge tubes and the black-brown reaction product was added. The nanocrystals were separated by centrifugation at 3000 rpm for 5 minutes. The brownish supernatant was decanted and the remaining nanocrystals were dissolved in chloroform resulting in a black-brown solution.

Table 8: used amounts of CIS nanocrystals and pyridine for ligand exchange

method	CIS [mg]	pyridine [ml]
4.1.1	207	5
4.1.2	150	5
4.1.4	150	5

4.2.2 Ligand exchange with 1-hexanethiol

A specific amount of nanocrystals, which were prepared as depicted in chapters 4.1.1, 4.1.2 and 4.1.4, was dissolved in 1-hexanethiol. After 24 hours, the solutions were left to cool down to room temperature. The precipitation agent (volume ratio of 10:1 to reaction product) was poured into two centrifuge tubes and the black-brown reaction product was added. The nanocrystals were separated by centrifugation at 3000 rpm for 5 minutes. The brownish supernatant was decanted and the remaining nanocrystals were dissolved in chloroform resulting in a black-brown solution. The exact values of CIS crystals and 1-hexanethiol used, the reaction parameters as well as the precipitation agents are listed in Table 9.

Table 9: amounts of CIS, 1-hexanethiol and precipitation reagents as well as reaction parameters used for ligand exchange

method	CIS [mg]	1-hexanethiol [ml]	CHCl$_3$ [ml]	T [°C]	precipitation agent
4.1.1	130	5	-	80	EtOH/acetone 1:1
4.1.2	150	5	-	80	EtOH/ acetone 1:1
4.1.4	150	5	-	80	EtOH/ acetone 1:1
4.1.4	200	4	-	80	EtOH/ acetone 1:1
4.1.4	130	3.2	-	80	EtOH/ acetone 1:1
4.1.4	333	6.66	-	120	EtOH/n-hexane 1:1
4.1.4	300	10	-	85	EtOH/ acetone 1:1
4.1.4	300	0.3	3	85	EtOH/ acetone 1:1

4.2.3 Ligand exchange with 1,3-benzenedithiol

ITO substrates, which were already coated with a polymer/CIS solution with 1-hexanethiol exchanged ligands (see 4.2.2 and 4.3.4.1), were sticked onto the inside wall of glass vials filled with 30 µl 1,3- benzenedithiol (BDT). The vials were closed and heated up to 120 °C in 20 minutes. The vapor of BDT caused a dissolution of the polymer/CIS layer. Consequently, this ligand exchanged was not further investigated.

4.2.4 Ligand exchange with t-butylthiol

175 mg CIS nanocrystals which were prepared as depicted in chapter 4.1.4 were dissolved in t-butylthiol. The reaction was performed at 80 °C. After 24 hours, the solutions were left to cool

down to room temperature. Pentane (volume ratio of 4:1 to reaction product) was poured into two centrifuge tubes and the black-brown reaction product was added. The nanocrystals were separated by centrifugation at 3000 rpm for 5 minutes. The brownish supernatant was decanted and the remaining nanocrystals were dissolved in chloroform resulting in a black-brown solution. Due to odor issues this approach was not further investigated.

4.2.5 Ligand exchange with ammonium thiocyanate

A specific amount of CIS nanocrystals, which were prepared as depicted in chapters 4.1.3 and 4.1.4, were mixed with a specific amount of ammonium thiocyanate dissolved in acetone. The brownish solution was agitated for around 1 minute and got slightly warm during mixing. For precipitation, the solution was poured into a centrifuge tube and the nanocrystals were separated by centrifugation at 3000 rpm for 5 minutes. A few milliliters of acetone were added to the nanocrystals, the suspension was again agitated for around 1 minute and centrifuged as described above. The clear supernatant was decanted and the remaining nanocrystals were dissolved resulting in a black-brown solution. The exact values of CIS particles and ammonium thiocyanate used, the concentration of the ammonium thiocyanate solution as well as the end concentration of the particles and their solvent are listed in Table 10.

Table 10: amounts of CIS and ammonium thiocyanate as well as solvent used for ligand exchange

method	CIS [ml]	NH_4SCN [ml]	NH_4SCN [mol/l]	solvent	final conc. [mg/ml]
4.1.3	2	2	0.26	DMF	not soluble
4.1.4	4	2	0.13	DMF	10
4.1.4	4	3 x 2	0.13	DMF	10
4.1.4	4	4	0.39	DMF	30

4.3 Preparation of solar cells

4.3.1 Cleaning of substrates

The conductive side of ITO covered glass substrates was determined using a multimeter and consequently the non-conductive side of the substrates was labeled with a glass pen with a consecutive number. The substrates were put into a beaker filled with isopropanol and sonicated in an ultrasonic bath for 10 minutes at 40 °C. Next, the substrates were removed from the isopropanol bath and dried with a stream of nitrogen gas.

4.3.2 Bulk heterojunction assembly

The substrates were cleaned as described in chapter 4.3.1. The surface of the substrates was activated using plasma etching and coated with PEDOT:PSS via spin coating at 3500 rpm for 30 seconds. To remove remaining solvent, the PEDOT:PSS covered substrates were tempered for 15 minutes at 150 °C. Afterwards, the substrates were transferred into the glove

box and the active layer was applied via spin coating at 1500 rpm for 20 seconds using 20 μl of polymer/CIS solution. Finally, 70-90 nm aluminum electrodes were applied via thermal evaporation. The devices were characterized by I/V measurements.

4.3.3 Quantum-dot sensitized solar cells

The substrates were cleaned as described in chapter 4.3.1. The surface of the substrates was activated using plasma etching. Afterwards the substrates are transferred into the glovebox and coated via spin coating with a solution of compact TiO_x precursor. 20 μl of the solution were applied on the devices at 4000 rpm with a velocity of 2000 rpm/s for 30 seconds. The coated glass substrates were put in a tube furnace at 470 °C for 45 minutes. Afterwards, the substrates were transferred into the glove box and coated via spin coating with a solution of titanium dioxide paste in terpineol. 20 μl of the solution were applied on the devices at various rpm and velocity for 30 seconds. The coated glass substrates were again put in a tube furnace at 470 °C for 45 minutes. Next, the substrates were transferred into the glove box. The nanocrystals were applied via spin coating at various velocities using 25 μl of the solution. Up to eleven films of nanocrystals were applied. A layer of P3HT with various concentration was applied on the substrates at 1500 rpm with a velocity of 1000 rpm/s for 20 seconds using 25 μl solution. Finally, electrodes consisting of 10 nm MoO_3 and 90 nm silver were applied using evaporation deposition. The devices were characterized by I/V measurements.

4.3.4 Preparation of active layer

4.3.4.1 Bulk heterojunction assembly

The polymer PCDTBT was dissolved in chlorobenzene reaching a concentration of 5 mg/ml. The solutions were stirred at 70 °C for one hour. The ligand exchanged CIS nanocrystals were dissolved in the polymer solution with a specific polymer to CIS ratio (wt:wt). The ratios 1:5, 1:9 and 1:15 of polymer to CIS were used.

4.3.4.2 Quantum-dot sensitized solar cells

Solutions of various polymers dissolved in chlorobenzene with different concentrations were prepared. The polymers as well as their concentrations can be taken from Table 11.

Table 11: polymers and their concentrations tested as hole transport layer

polymer	concentrations [mg/ml]
PCDTBT	15; 25; 30
P3HT	15; 25; 30
Spiro-OMeTAD	see below

For the Spiro-OMeTAD solution 17.2 mg (70 mmol) Spiro-OMeTAD, 2.2 mg (35 mmol) LiTFSI, 0.63 mg (2.1 mmol) FK 209 Co(III) TFSI and 1.25 μl (23 mmol) tributyl phosphate were dissolved in 200 μl chlorobenzene.

4.3.5 Preparation of precursor for compact TiO$_x$ films

For the preparation of the compact TiO$_x$ films a precursor solution was prepared by mixing 70 µl titanium isopropoxide, 55 µl ethanolamine and 1 ml 2-methoxyethanol in a glass vial and stirring until the constituents were mixed well.

4.3.6 Preparation of precursor for mesoporous TiO$_x$ layers

For the preparation of the mesoporous TiO$_x$ layers a precursor solution was prepared by mixing 1.00 g of a titanium dioxide paste with 2.695 ml terpineol in a glass vial and stirring overnight.

4.4 Characterization methods and devices

4.4.1 X-Ray diffraction measurements

The X-Ray diffraction measurements were conducted on a Siemens D501 diffractometer in Bragg–Brentano geometry operated at 40 kV and 30 mA, using Cu Kα radiation and a graphite monochromator at the secondary side. The measurements were performed by Birgit Kunert.

4.4.2 UV/Vis measurements

The absorption of different layers was measured between 300 nm and 1000 nm using a PerkinElmer Lambda 35 UV/VIS spectrometer.

For the determination of the band gap of the CIS nanocrystals, a solution of the particles dissolved in chloroform was drop coated onto glass substrates and dried overnight.

For the measurement of the PCDTBT and the PCDTBT/CIS layers, a solution of 5 mg/ml polymer in chlorobenzene was prepared. A polymer to CIS ratio of 1:5, 1:9 and 1:15 was used. Glass substrates were cleaned as described in 4.3.1 and the active layer was applied on the substrates at 1000 rpm with a velocity of 1500 rpm/s for 20 seconds using 25 µl solution.

For the measurement of the P3HT/CIS layers, glass substrates were cleaned as described in 4.3.1. The substrates were coated via spin coating with a solution of titanium dioxide paste in terpineol. 20 µl of the solution were applied on the devices at 3000 rpm and a velocity of 6000 rpm/s for 30 seconds. The coated glass substrates were put in a tube furnace at 470 °C for 45 minutes. Next, the substrates were transferred into the glove box. The nanocrystals were applied via spin coating at 500 rpm and a velocity of 800 rpm/s for 30 seconds using 25 µl of the solution. Up to eleven films of nanocrystals were applied. A layer of P3HT with a concentration of 30 mg/ml was applied on the substrates at 1500 rpm with a velocity of 1000 rpm/s for 20 seconds using 25 µl solution.

4.4.3 Thermogravimetric analysis

Thermo-gravimetric analyses were performed on a Netzsch Jupiter 449 C simultaneous thermal analyzer. The measurements were carried out under helium atmosphere at a heating

rate of 10 °C/min. The samples were measured between room temperature and 550 °C. The analysis was performed by Amtsrätin Ing. Josefine Hobisch.

4.4.4 Infrared spectroscopy

FT-IR spectra were gained using a Bruker Alpha FT-IR spectrometer. All FT-IR spectra of the CIS nanocrystals were recorded in attenuated total reflection (ATR) mode in the spectral range between 4000 and 400 cm^{-1}.

4.4.5 NMR spectroscopy

NMR spectroscopy (^{1}H, ^{13}C) was performed on a Bruker Avance 300 MHz spectrometer. Deuterated solvents (CDCl$_3$) were obtained from Cambridge Isotope Laboratories Inc.

4.4.6 I/V characteristics measurements

The prepared solar cell substrates were put in a custom-made box in the glove box. The electrical contacts of the measurement box were connected to a Keithley 2400 source measurement unit. For validation of the light intensity the measurement box contained a photo diode. The solar cells were measured under an illumination of 1000 W/m² and in the dark. The light was generated by a tungsten halogen lamp. The Keithley 2400 was connected to a computer where the measurement was accomplished by a Labview program. The voltage was changed from 2 V to -0.5 V.

EQE spectra were performed using a AMKO MuLTImode4 monochromator equipped with a Xenon lamp and a Keithley 2400 source meter.

4.4.7 Layer thickness measurements

The thickness of the layers on the solar cell substrates was determined by a Bruker Dektak XT profilometer. A scratch was made into the film with a scalpel to enable the measurement. With a thin needle the profile of the surface of the scratch and the whole layer was measured. The film thickness was determined as the difference in height between the active layer and the uncovered ITO layer. The thickness of a device was measured on three to five different positions to obtain more accurate results.

4.4.8 Photoluminescence quenching experiments

For the determination of the photoluminescence quenching of the PCDTBT/CIS system without any ligand exchange 2.5 cm x 2.5 cm glass substrates were cleaned as described in chapter 4.3.1. Next, the substrates were coated via spin coating with a solution of ZnO nanocrystals dissolved in chlorobenzene with a concentration of 25 mg/ml at 2000 rpm with a velocity of 2000 rpm/s for 20 seconds using 50 µl solution. The active layer was applied via spin coating at 1500 rpm for 20 seconds using 50 µl of polymer/CIS solution. The solution of the active layer

was prepared as described in chapter 4.3.4.1. Here, ZnO nanoparticles were used due to a better adhesion of the CIS nanocrystals without ligand exchange on the substrates.

For the determination of the photoluminescence quenching of the PCDTBT/CIS system with 1-hexanethiol exchange 2.5 cm x 2.5 cm glass substrates were prepared as described in chapter 5.3.1. The nanocrystals, which were prepared as depicted in chapter 4.1.4 and ligand exchanged as described in chapter 4.2.2, were used for the measurement. The solution of the active layer was prepared as described in chapter 4.3.4.1.

The measurements were done in ambient atmosphere on a Horiba Scientific FluoroLog 3 spectrofluorometer equipped with a NIR-sensitive Hamamatsu R2658 photomultiplier. An excitation wavelength of 565 nm was used and the spectra were measured from 580 to 950 nm at a slid with of 3 nm.

4.4.9 Transmission Electron Microscopy

Solutions of nanocrystals dissolved in chloroform, which were prepared as described in chapter 4.1.4, were diluted with chloroform. The volume ratios of dilution were 1:10, 1:50 and 1:100.

For transmission electron microscopy, samples were prepared by dropping a solution of nanocrystals dissolved in chloroform onto a nickel-TEM-grid (Quantifoil) with a carbon film and subsequent evaporation of the solvent at room temperature. TEM images as well as EDX spectra were gained on a Tecnai F20 microscope (FEI Company) equipped with a Schottky emitter, an energy dispersive X-ray spectrometer as well as a high resolution Gatan imaging filter with an UltraScanCCD camera. TEM measurements were performed by DI Dr. Karin Wewerka and DI Dr. Ilse Letofsky-Papst at the Institute for Electron Microscopy and Nanoanalysis (FELMI) at Graz University of Technology.

4.4.10 Synthesis reactor

The syntheses described in chapters 4.1.8 and 4.1.9 were synthesized in the synthesis reactor Monowave 50 from Anton Paar. The following heat program was used: 25 °C to 100 °C in 10 min, 100 °C to 200 °C in 99 min and holding 200 °C for 60 min. At the end the reaction mixture was cooled to 40 °C.

4.5 Chemicals, materials, solvents

All chemicals, materials and solvents which were used for the syntheses and the preparation of the solar cells, their purity and source of supply are listed in Table 12.

Table 12: Chemicals, materials and solvents used for syntheses and preparation of solar cells

Chemical/material/solvent	Source of supply	Purity/properties
1,2,4-Trichlorobenzene	Aldrich	99%, anhydrous
1-Dodecanethiol	Fluka	≥97%
1-Hexanethiol	Aldrich	95%
1-Octadecene	Aldrich	90%
Acetone	Sigma Aldrich	puriss; ≥99% (GC)
Aluminum	Kurt J. Lesker	99.99%
Ammonium thiocyanate	Merck KGaA	for analysis
Chlorobenzene	Aldrich	99.9% (for HPLC)
Chloroform	VWR Chemicals	stabilized with ≈ 0.6% ethanol
Copper acetate	Aldrich	97%
Copper xanthate	Aglycon	Charge: Sept. 2011
Dimethylformamide	Sigma Aldrich	puriss. ≥99.8% (GC)
Ethanol	TU Graz	puriss.
n-Hexane	Roth	95%
Indium acetate	Aldrich	99.99%
Indium xanthate	Aglykon	Charge: Nov. 2011
Isopropanol	Roth	≥99.8%
Methanol	TU Graz	puriss.
Molybdenum(VI) oxide	Aldrich	99.98%
Oleic acid	Aldrich	90%
Oleyl amine	Acros organics	≈ C18 content 80-90%
PCDTBT	1-Material Inc.	medium (OS0502)
PEDOT:PSS	Heraeus	Clevios P VP. Al4083
Pentane	TU Graz	puriss.
Pyridine	Aldrich	≥99%
Silver	Kurt J. Lesker	99.99%
t-Dodecanethiol	Aldrich	mixture of isomers, 98.5%
Terpineol	Aldrich	mixture of isomers, anhydrous
Titanium oxide paste	Dyesol	Batch 426
Trioctylphosphine oxide	Aldrich	99%

5 Summary and Outlook

The aim of this thesis was to synthesize $CuInS_2$ nanocrystals via colloidal methods and their characterization. Ligand exchange should be performed and thereafter the nanocrystals introduced into nanocomposite and quantum-dot sensitized solar cells, respectively.

The synthesis of CIS nanocrystals, which was performed using CuAc and $In(Ac)_3$ as precursors, oleylamine as solvent and *tert*-dodecanethiol and 1-dodecanethiol as capping agents, yielded CIS nanocrystals. Although out of the measured XRD pattern it was derived that the crystal structure of the nanocrystals is a mixture of the wurtzite and the chalcopyrite structure instead of the desired chalcopyrite structure. Therefore, a new synthesis method was developed.

The developed synthesis method using copper and indium xanthate as precursor and oleylamine and oleic acid as solvent and capping agent yielded CIS nanocrystals with the desired chalcopyrite structure. Whereas the capping agent turned out to be a product of both capping agents, namely dioleamide.

Due to a rather small size of the nanocrystals several variations of the synthesis method using the metal xanthates were tested. The capping agents were changed to oleic acid, a mixture of octadecene and oleylamine and a different mixture of oleyl amine to oleic acid. Also controlled heating of the reaction mixture was investigated. Except for the synthesis with pure oleic acid no other method provided particles with a higher diameter. The drawback of the oleic acid capped particles was their insufficient solubility in chloroform and chlorobenzene. Therefore, further experiments were done with the particles capped with dioleamide.

For a verification of the synthesized $CuInS_2$ nanocrystals before their incorporation in hybrid solar cells their band gap was determined. Compared to literature the value of 1.57 eV was in an optimal range.

Out of several different compounds tested for ligand exchange 1-hexanethiol and ammonium thiocyanate turned out to be promising options. The success of the ligand exchanges themselves was satisfying which could be seen in the infrared spectroscopy measurements and the thermogravimetric analyses. Nearly all former ligand could be exchanged with the new ligands.

Before introducing 1-hexanethiol nanocrystals as acceptor material into nanocomposite solar cells the active layer in combination with the conductive polymer PCDTBT as donor material was analyzed. UV/Vis spectroscopy, which was conducted of active layers with different polymer to nanocrystal ratios, surprisingly did not show a coherence of the absorbance with increasing nanocrystal content. The layer with the highest amount of nanocrystals had the lowest absorption. Photoluminescence quenching experiments showed that charge transfer

works much better with the nanocrystals where ligand exchange was conducted compared to the non-exchanged nanocrystals. Also with increasing content of nanocrystals the quenching of the photoluminescence was increased further.

Polymer/nanocrystal solar cells were prepared using 1-hexanethiol nanocrystals and PCDTBT. The prepared devices showed a good performance. After optimizing the ratio of polymer to nanocrystals to 1:9 and the thickness of the active layer to around 92 nm an improve in performance was achieved. Annealing of the active layer did not provide an improvement in performance.

Quantum-dot sensitized solar cells were prepared with thiocyanate capped nanocrystals as light absorber and P3HT as hole transport layer. Various other polymers were tested, but their performance was worse than P3HT. The thickness of mesoporous TiO_x as well as the concentration of P3HT were optimized before the incorporation of the nanocrystals in the solar cells. A thickness of mesoporous TiO_x of around 160 nm and a concentration of P3HT of 30 mg/ml in chlorobenzene delivered the highest values.

Different thicknesses of nanocrystal layers from one to eleven layers were investigated. UV/Vis spectroscopy showed a slight increase of the absorbance with nanocrystal content, but the overall absorbance was very small. After coating the polymer layer the absorbance of the pure polymer was slightly increased.

Quantum-dot sensitized solar cells with one, three and five layers of nanocrystals in DMF were prepared. The best performance provided the substrates with five layers whereas after 24 hours the substrates with only one layer had the best performance. This might be due to a bigger interface between the nanocrystals and the polymer.

The influence of annealing on the overall performance was tested. Against expectations no improvement was made. It was supposed that the solvent for the nanocrystals would disturb the charge transfer and therefore an annealing step would increase the performance.

As a second step a treatment with $InCl_3$ was done. Herewith redundant sulfur should be bound and vacancies should be filled out with InS_3. The performance could also not be influenced by this treatment.

The EQE measurements showed that the efficiency of the solar cells, which were expected to be quantum-dot sensitized, only contributes to the polymer P3HT. It can be concluded that quantum-dot sensitized solar cells could not be prepared successfully.

Further research should be directed towards finding a possibility to control the growth of the nanocrystals when using metal xanthates as precursors or search on new precursors. Additionally, optimization should be done when using thiocyanate as ligand and incorporating those nanocrystals in quantum-dot sensitized solar cells. However, in the last years a lot of

research was done in the field of $CuInS_2$ nanocrystals and their application in hybrid solar cells. For nanocomposite solar cells using $CuInS_2$ synthesized by the colloidal method no reports with efficiencies above 1% were published until now. Rath et al.[26] accomplished to reach efficiencies of 2.8%, but they used the in-situ route for preparing the nanocrystals. So further research should be directed towards improving the ligand exchange of $CuInS_2$ nanocrystals or towards improving the nanocrystals itself.

6   Abbreviations

CIS	copper indium disulfide
Cu-Hep	copper O-2,2-dimethylpentan-3-yl dithiocarbonate
DDT	dodecanethiol
EQE	external quantum efficiency
FF	fill factor
HOMO	highest occupied molecular orbital
In-Hep	indium O-2,2-dimethylpentan-3-yl dithiocarbonate
I_{SC}	short circuit current
ITO	indium tin oxide
LUMO	lowest unoccupied molecular orbital
OA	oleic acid
OAm	oleyl amine
ODE	octadecene
P3HT	poly(3-hexylthiophene-2,5-diyl)
PCDTBT	poly[N-9'-heptadecanyl-2,7-carbazole-alt-5,5-(4',7'-di-2-thienyl-2',1',3'-benzothiadiazole)]
PCE	power conversion efficiency
PEDOT:PSS	poly(3,4-ethylenedioxythiophene)-poly(styrenesulfonate)
Spiro-OMeTAD	2,2',7,7'-Tetrakis-(N,N-di-4-methoxyphenylamino)-9,9'-spirobifluorene
TGA	thermogravimetric analysis
TOPO	trioctylphosphine oxide
V_{OC}	open circuit voltage
XRD	X-ray diffraction

7   Literature

(1)   U.S. Energy Information Administration. *International Energy Outlook 2017*; 2017.

(2)   Caetano, N. S.; Mata, T. M.; Martins, A. A.; Felgueiras, M. C. *Energy Procedia* **2017**, *107*, 7–14.

(3)   Moulé, A. J.; Chang, L.; Thambidurai, C.; Vidu, R.; Stroeve, P. *J. Mater. Chem.* **2012**, *22*, 2351–2368.

(4)   Solar energy https://www.bp.com/en/global/corporate/energy-economics/statistical-review-of-world-energy/renewable-energy/solar-energy.html (accessed Oct 31, 2017).

(5)   Rath, T.; Trimmel, G. *Hybrid Mater.* **2014**, *1* (1), 15–36.

(6)   Yoon, W. In *Photovoltaic Solar Energy: From Fundamentals to Applications*; Wiley-VCH, 2017.

(7)   Mertens, K. *Photovoltaik: Lehrbuch zu Grundlagen, Technologie und Praxis*; Carl Hanser Verlag, 2011.

(8)   Kittel, C. *Introduction to Solid State Physics*, 8th ed.; Wiley-VCH, 2005.

(9)   Green, M. A.; Emery, K.; Hishikawa, Y.; Warta, W.; Dunlop, E. D. *Prog. Photovoltaics Res. Appl.* **2016**, *24*, 905–913.

(10)   Wright, M.; Uddin, A. *Sol. Energy Mater. Sol. Cells* **2012**, *107*, 87–111.

(11)   Güneş, S.; Sariciftci, N. S. In *Printable Solar Cells*; Scrivener Publishing LLC, 2017; 3–36.

(12)   Balazs, D. M.; Speirs, M. J.; Loi, M. A. In *Organic and Hybrid Solar Cells*; Huang, H., Huang, J., Eds.; Springer International Publishing, 2014; pp 301–337.

(13)   Greenham, N. C.; Peng, X.; Alivisatos, A. P. *Phys. Rev. B* **1996**, *54* (24), 17628–17637.

(14)   Liu, Z.; Sun, Y.; Yuan, J.; Wei, H.; Huang, X.; Han, L.; Wang, W.; Wang, H.; Ma, W. *Adv. Mater.* **2013**, *25*, 5772–5778.

(15)   Eck, M.; Krueger, M. In *Organic Photovoltaics: Materials, Device Physics, and Manufacturing Technologies*; Wiley-VCH, 2014; pp 171–208.

(16)   O'Regan, B.; Grätzel, M. *Nature* **1991**, *353*, 737–740.

(17)   Docampo, P.; Guldin, S.; Leijtens, T.; Noel, N. K.; Steiner, U.; Snaith, H. J. *Adv. Mater.* **2014**, *26*, 4013–4030.

(18)   Freitag, M.; Boschloo, G. *Curr. Opin. Electrochem.* **2017**, *2*, 111–119.

(19)   Tennakone, K.; Kumara, G. R. R. A.; Kumarasinghe, A. . R.; Wijayantha, K. G. U.; Sirimanne, P. M. *Semicond. Sci. Technol.* **1995**, *10*, 1689–1693.

(20)   Sharma, D.; Jha, R.; Kumar, S. *Sol. Energy Mater. Sol. Cells* **2016**, *155*, 294–322.

(21)   Rogach, A. L. *Semiconductor nanocrystal quantum dots: synthesis, assembly, spectroscopy and applications*; Springer Verlag, 2008.

(22)   Fradler, C.; Rath, T.; Dunst, S.; Letofsky-Papst, I.; Saf, R.; Kunert, B.; Hofer, F.; Resel, R.; Trimmel, G. *Sol. Energy Mater. Sol. Cells* **2014**, *124*, 117–125.

(23)   Kolny-Olesiak, J.; Weller, H. *ACS Appl. Mater. Interfaces* **2013**, *5* (23), 12221–12237.

(24)   Leach, A. D. P.; Macdonald, J. E. *J. Phys. Chem. Lett.* **2016**, *7* (3), 572–583.

(25)   Buchmaier, C.; Rath, T.; Pirolt, F.; Knall, A.-C.; Kaschnitz, P.; Glatter, O.; Wewerka,
        K.; Hofer, F.; Kunert, B.; Krenn, K.; Trimmel, G. *RSC Adv.* **2016**, *6* (108), 106120–
        106129.

(26)   Rath, T.; Edler, M.; Haas, W.; Fischereder, A.; Moscher, S.; Schenk, A.; Trattnig, R.;
        Sezen, M.; Mauthner, G.; Pein, A.; Meischler, D.; Bartl, K.; Saf, R.; Bansal, N.; Haque,
        S. A.; Hofer, F.; List, E. J. W.; Trimmel, G. *Adv. Energy Mater.* **2011**, *1* (6), 1046–
        1050.

(27)   Arici, E.; Sariciftci, N. S.; Meissner, D. *Adv. Funct. Mater.* **2003**, *13* (2), 165–170.

(28)   Panthani, M. G.; Akhavan, V.; Goodfellow, B. W.; Schmidtke, J. P.; Dunn, L.;
        Dodabalapur, A.; Barbara, P. F.; Korgel, B. a. **2008**, *130*, 16770–16777.

(29)   Method, F. S. *Cryst. Growth Des.* **2010**, *8* (7), 2402–2405.

(30)   Kruszynska, M.; Borchert, H.; Parisi, J.; Kolny-Olesiak, J. *J. Nanoparticle Res.* **2011**,
        13 (11), 5815–5824.

(31)   Santra, P. K.; Nair, P. V.; George Thomas, K.; Kamat, P. V.; Sensitized, C.; Dot, Q.;
        Cell, S.; Dynamics, E.; Performance, P. *J. Phys. Chem. Lett.* **2013**, *4*, 722–729.

(32)   Fafarman, A. T.; Koh, W. K.; Diroll, B. T.; Kim, D. K.; Ko, D. K.; Oh, S. J.; Ye, X.;
        Doan-Nguyen, V.; Crump, M. R.; Reifsnyder, D. C.; Murray, C. B.; Kagan, C. R. *J. Am.
        Chem. Soc.* **2011**, *133* (39), 15753–15761.

(33)   Greaney, M. J.; Brutchey, R. L. *Mater. Today* **2015**, *18* (1), 31–38.

(34)   Zhou, Y.; Riehle, F. S.; Yuan, Y.; Schleiermacher, H.-F.; Niggemann, M.; Urban, G. A.;
        Krüger, M. *Appl. Phys. Lett.* **2010**, *96*, 13304.

(35)   Rath, T.; Kaltenhauser, V.; Haas, W.; Reichmann, A.; Hofer, F.; Trimmel, G. *Sol.
        Energy Mater. Sol. Cells* **2013**, *114*, 38–42.

(36)   Radychev, N.; Scheunemann, D.; Kruszynska, M.; Frevert, K.; Miranti, R.; Kolny-
        Olesiak, J.; Borchert, H.; Parisi, J. *Org. Electron. physics, Mater. Appl.* **2012**, *13* (12),
        3154–3164.

(37)   Bu, W.; Chen, Z.; Chen, F.; Shi, J. *J. Phys. Chem. C* **2009**, *113* (28), 12176–12185.

(38)   Asgary, S.; Mirabbaszadeh, K.; Nayebi, P.; Emadi, H. *Mater. Res. Bull.* **2014**, *51*, 411–
        417.

(39)   Mudryi, A. V.; Victorov, I. A.; Gremenok, V. F.; Patuk, A. I.; Shakin, I. A.; Yakushev, M.
        V. *Thin Solid Films* **2003**, *431–432* (3), 197–199.

(40)   Fischereder, A.; Rath, T.; Haas, W.; Amenitsch, H.; Albering, J.; Meischler, D.;
        Larissegger, S.; Edler, M.; Saf, R.; Hofer, F.; Trimmel, G. *Chem. Mater.* **2010**, *22* (11),
        3399–3406.

(41)   Rockett, A. A. *Curr. Opin. Solid State Mater. Sci.* **2010**, *14* (6), 143–148.

(42)   Guan, R.; Wang, X.; Sun, Q. *J. Nanomater.* **2015**, *2015*, 1–8.

(43)   Omata, T.; Nose, K.; Otsuka-Yao-Matsuo, S. *J. Appl. Phys.* **2009**, *105* (7).

(44)   Calatayud, D. G.; Jardiel, T.; Rodríguez, M.; Peiteado, M.; Fernández-Hevia, D.;
       Caballero, A. C. *Ceram. Int.* **2013**, *39* (2), 1195–1202.

(45)   Socrates, G. *Infrared characteristic group frequencies: Tables and Charts*, 2nd ed.;
       Wiley, 1998.

8 List of Figures

9   List of Tables